

# **Shared Decision-Making and Control Between Humans and Adaptive Control Algorithms**

by

Benjamin T. Thomsen

B.Eng., McGill University (2015)

Submitted to the Department of Mechanical Engineering  
in partial fulfillment of the requirements for the degree of

Master of Science

at the

MASSACHUSETTS INSTITUTE OF TECHNOLOGY

June 2018

© Massachusetts Institute of Technology 2018. All rights reserved.

Author .....  
Department of Mechanical Engineering  
May 11, 2018

Certified by .....  
Anuradha M. Annaswamy  
Senior Research Scientist  
Thesis Supervisor

Accepted by .....  
Rohan Abeyaratne  
Chairman, Department Committee on Graduate Theses



# **Shared Decision-Making and Control Between Humans and Adaptive Control Algorithms**

by

Benjamin T. Thomsen

Submitted to the Department of Mechanical Engineering  
on May 11, 2018, in partial fulfillment of the  
requirements for the degree of  
Master of Science

## **Abstract**

In this thesis we consider the problem of controlling a dynamical system subject to both parametric uncertainties and the sudden occurrence of severe changes in the dynamic architecture of the system. These anomalies, including the introduction of unmodeled linear dynamics or time delays, present difficulties in control for both human operators and autonomous model-based control algorithms. Online adjustment to asymptotically reject the effect of parametric uncertainty is possible through the proper use of adaptive control, and to a certain extent is paralleled by human learning and adaptation in manual control. Changes to the dynamic structure of the system, however, may lead to poor closed-loop performance and instability whether the control loop is being closed by a human or adaptive control algorithm.

We introduce a shared decision-making and control framework based on adaptive control which gives supervisory human operators a targeted responsibility in the mitigation of dynamical anomalies and enables the recovery of closed-loop system stability and command tracking performance without transferring control responsibilities to the human operator. This shared controller is defined in this thesis for systems with full-state feedback as well as output feedback only. Anomaly response with shared control is demonstrated on an unmanned aerial vehicle, whose actuators suddenly change from first-order to second-order.

Thesis Supervisor: Anuradha M. Annaswamy  
Title: Senior Research Scientist



## Acknowledgments

First and foremost, I would like to thank my advisor, Dr. Anuradha Annaswamy. In my time at MIT she has taught me everything I know about control theory, and has given me the mindset needed to teach myself when I come across unfamiliar subjects. She provided the support and direction I needed to succeed in this research. I appreciate all the time she has devoted to answering my questions and clearing all the hurdles for this work to progress. I would like to thank Dr. Eugene Lavretsky for the conversations which have shaped my research and inspired me to think about the practical aspects of control design.

I would like to thank all my labmates in the Active Adaptive Control Laboratory for their support throughout this research. I would like to thank Max Zheng Qu in particular – although we barely overlapped at MIT, Max’s advancements in adaptive control theory paved the way for this thesis, and his code repository for simulations saved me countless hours of implementation for MIMO adaptive control. Heather Hussain’s advice and support with my questions is greatly appreciated. Joey and Bitzy have been invaluable resources to bounce ideas off. Thank you all for the time you set aside to help me with this research.

I am grateful to the support and inspiration of my friends throughout my time at MIT. Finally, I’d like to thank my parents for inspiring my passion for science and engineering, and for happily providing me with excuses to take a break from working.



# Contents

<b>1</b>	<b>Introduction</b>	<b>15</b>
1.1	Background . . . . .	16
1.2	Contributions . . . . .	19
<b>2</b>	<b>Problem Statement</b>	<b>21</b>
2.1	Onboard Human Pilot and Full-State Feedback Adaptive Control . .	21
2.1.1	Actuator Fault . . . . .	23
2.1.2	Time-Delayed Sensor Measurements . . . . .	23
2.2	Remote Human Operation and Output Feedback Adaptive Control .	25
2.2.1	Actuator Fault . . . . .	25
<b>3</b>	<b>Shared Control with Human Pilot and State Feedback</b>	<b>29</b>
3.1	The Proposed Shared Controller . . . . .	29
3.1.1	Role of the Human Pilot . . . . .	30
3.1.2	MRAC-Based Adaptive Autopilot . . . . .	31
3.1.3	The Overall Shared Controller . . . . .	34
<b>4</b>	<b>Shared Control with Remote Human Pilot and Output Feedback</b>	<b>37</b>
4.1	Adaptive Output-Feedback Control . . . . .	38
4.1.1	Nominal Adaptive Control Design . . . . .	39
4.1.2	Recovery Adaptive Control Design . . . . .	41
4.2	Human Supervisor . . . . .	45

<b>5 Anomaly Response Simulations</b>	<b>47</b>
5.1 State Feedback . . . . .	47
5.1.1 Actuator Fault . . . . .	48
5.1.2 Time-Delayed Sensor Measurements . . . . .	51
5.2 Output Feedback . . . . .	55
5.2.1 HALE Aircraft Model . . . . .	55
5.2.2 Numerical Simulations and Results . . . . .	59
<b>6 Concluding Remarks</b>	<b>69</b>
<b>A Tables</b>	<b>71</b>

# List of Figures

1-1	General shared decision-making and control architecture adapted from Ref. [?] . . . . .	18
2-1	Supervisory operation of a fleet of HALE UAVs . . . . .	26
3-1	Block diagram of model-reference adaptive controller with closed-loop reference model . . . . .	33
3-2	Our proposal for shared decision making following an anomaly, with stages of decision making categorized in Ref. [?] . . . . .	35
5-1	Command ( $r$ ) and output ( $\phi$ ): under nominal operation ( $t \leq 30$ s), after the change in actuator dynamics ( $30 < t \leq 90$ s), and after a corrective action to switch the controller ( $t > 90$ s) . . . . .	49
5-2	Adaptive feedback gains for the same simulation example as in Figure 5-1: under nominal operation ( $t \leq 30$ s), after the change in actuator dynamics ( $30 < t \leq 90$ s), and after a corrective action to switch the controller ( $t > 90$ s) . . . . .	50
5-3	The tracking error $e$ for the same simulation example as in Figure 5-1: under nominal operation ( $t \leq 30$ s), after the change in actuator dynamics ( $30 < t \leq 90$ s), and after a corrective action to switch the controller ( $t > 90$ s) . . . . .	50
5-4	Unit step responses for closed-loop transfer functions at different stages of simulation in case (i), demonstrating performance improvement after corrective action . . . . .	51

5-5	Command ( $r$ ) and output ( $\phi$ ): under nominal operation ( $t \leq 30$ s), after the sudden addition of a time delay ( $30 \text{ s} < t \leq 90$ s), and after a corrective action to switch the controller ( $t > 90$ s) . . . . .	53
5-6	Adaptive feedback gains for the same simulation example as in Figure 5-5: under nominal operation ( $t \leq 30$ s), after the sudden addition of a time delay ( $30 \text{ s} < t \leq 90$ s), and after a corrective action to switch the controller ( $t > 90$ s) . . . . .	53
5-7	The tracking error $e$ for the same simulation example as in Figure 5-5: under nominal operation ( $t \leq 30$ s), after the sudden addition of a time delay ( $30 \text{ s} < t \leq 90$ s), and after a corrective action to switch the controller ( $t > 90$ s) . . . . .	54
5-8	Unit step responses for closed-loop transfer functions at different stages of simulation in case (ii), demonstrating performance improvement after corrective action . . . . .	54
5-9	Rendering of very flexible aircraft model . . . . .	55
5-10	Poles of linearized system for different dihedral angles . . . . .	57
5-11	Dominant poles of linearized system, which move into the right-half complex plane when $\eta > 11^\circ$ . . . . .	58
5-12	Actuator trim at different dihedral angles . . . . .	58
5-13	Nom-1 simulation: RSLQR with no uncertainty in the control model	60
5-14	Nom-2 simulation: RSLQR with uncertainties $\Theta_p$ , $\Lambda_p$ , and $\Theta_1$ . . .	61
5-15	Nom-3 simulation: RSLQR + MRAC with uncertainties $\Theta_p$ , $\Lambda_p$ , and $\Theta_1$	62
5-16	AR-1 simulation: passive response to dynamical anomaly results in structural failure after 6 minutes . . . . .	64
5-17	AR-1 simulation: adaptive parameters diverge as controller struggles to adapt to unmodeled dynamics . . . . .	64
5-18	AR-1 simulation: model-following output error and command tracking error grow due to anomalous dynamics . . . . .	65
5-19	AR-3 simulation: shared response to the dynamical anomaly results in recovery of vehicle performance . . . . .	66

5-20 AR-3 simulation: the change in control model at $t = 800s$ stops the divergence of adaptive parameters . . . . .	66
5-21 AR-3 simulation: the change in control model at $t = 800s$ stops the error growth seen after the anomaly . . . . .	67



# List of Tables

A.1 Armadillos . . . . .	71
--------------------------	----



# Chapter 1

## Introduction

Model-based feedback control techniques, where control design is carried out based on *a priori* knowledge of system dynamics, have become ubiquitous in industries such as aerospace, due to their ability to specify characteristics of the closed-loop system dynamics, ensure stability, and certify optimality over a range of operating conditions. In any complex dynamical system, however, uncertainty is inevitable. Uncertainties may be present for myriad reasons including modeling errors, environmental variations, unforeseen anomalies, and disturbances. The field of adaptive control addresses a limitation of control based on models of plant dynamics, namely that parameters used to model the plant may be uncertain. Model reference adaptive control (MRAC) [?, ?] accommodates these parametric uncertainties through online tuning of control parameters to ensure specified closed-loop dynamics are realized. Recent advances in MRAC have included the development of closed-loop reference models (CRMs) [?], which greatly improves transient performance during online learning. Guarantees of stability and tracking convergence are obtained under a few assumptions on the underlying modeling structure. One such assumption includes knowing the order of the system *a priori* for control design. This in turn is used to determine the number of adjustable parameters which in turn represent the key adaptive elements of an adaptive controller.

Human operators of dynamical systems also develop mental models of expected dynamic behavior, often over long periods of active learning. Human pilots, for exam-

ple, have been modeled and studied extensively to examine their use of information feedback and ability to adapt their control strategies to unfamiliar situations [?, ?], and are found to have limits when attempting to rapidly learn unfamiliar and anomalous vehicle dynamics [?, ?, ?, ?, ?]. In stressful situations, human pilots tend to apply high control gains, which coupled with certain dynamical anomalies increases the risk of loss of control [?]. A recent study found that the majority of transport aircraft loss of control incidents over a 15-year period involved inaction or improper action by the flight crew [?]. Endsley (1996) points to pilot error following a transition from autonomous to manual control (often as the result of an anomaly) as a common factor in loss of control incidents [?]. Issues with manual control of dynamical systems are exacerbated when the human operator is physically separated from the dynamics of the system, as is the case with remotely piloted vehicles [?, ?]. The additional complexities involved with remote operation include a lack of sensory and perceptive cues regarding the plant state and its environment, time delays between the dynamical system and operator for both sensing and actuation, and difficulty ascertaining the open-loop dynamical response between control input and plant output [?].

This naturally leads one to address the problem of how the limitations of autonomous control systems based on adaptive control algorithms (as in Refs. [?] and [?]) and those of the human operators can be overcome by sharing decision-making and control tasks between adaptive control algorithms and human operators. The goal of this work is to develop one such framework where a supervisory human operator takes a targeted and active role in response to anomalous plant behavior, allowing an adaptive control algorithm to suitably adapt to the introduction of severe unmodeled dynamics and recover closed-loop control performance.

## 1.1 Background

Analysis of manual (human) control [?, ?, ?, ?] has been studied extensively in the flight control literature. The widely used crossover model of the human pilot in manual flight control[?] hypothesizes that the human pilot generates either lead or lag

equalization so that the open-loop transfer function of the pilot-vehicle system has the characteristics of a first-order system near the crossover frequency. For a plant (the aircraft) with dynamics  $Y_c(s)$ , the pilot would aim to provide lead equalization so that together with the pilot's dynamics  $Y_p(s)$ , an open-loop pilot-vehicle transfer function is generated as  $Y_{ol}(s) = Y_p(s)Y_c(s) = \frac{K}{s}e^{-\tau s}$  [?]. Assuming that the dominant characteristics of the aircraft are approximated by a second-order system and a pilot's action is in the form of a proportional-derivative (PD) controller, such a characteristic near the crossover frequency is reasonable to expect. More recent research has investigated pilot adaptation to time-varying dynamics in Refs. [?] and [?] and it has been argued that an adaptive PD controller with time-varying gains can be attributed to a pilot's actions. Zaal and Sweet [?] applied maximum-likelihood estimation (MLE) techniques to identify the time-varying parameters of pilots, whose gains correspond to that of an adaptive PD controller. In Ref. [?], the author used this technique to identify these parameters in a data set in which trained aircraft pilots in a simulation environment controlled multi-axis tasks undergoing a sudden and unexpected change in dynamics. Control performance in these experiments was shown to degrade after a change in vehicle dynamics to something with which the pilots were not familiar, even as the pilots adapted their feedback gains to try and recover their performance.

To maximize the probability of detection of an anomaly while minimizing the probability of false alarm, it may be advantageous to include the human operator in fault detection and diagnosis [?]. In particular, given that the anomaly response consists broadly of (a) perception of the anomaly, and (b) mitigation of the anomaly effects through suitable correction and compensation, the question is if a human operator can perform step (a) and model reference adaptive control algorithms can be used to perform step (b). Unlike Refs. [?] and [?] where the pilot performs both steps (a) and (b), we propose a shared control action where a perception task is performed by the pilot, while an adaptive autopilot compensates for the effect of anomaly. This task allocation can be thought of as a specific example of supervisory control, defined by Sheridan [?, ?]. The supervisory control structure of Ref. [?], modified for relevance

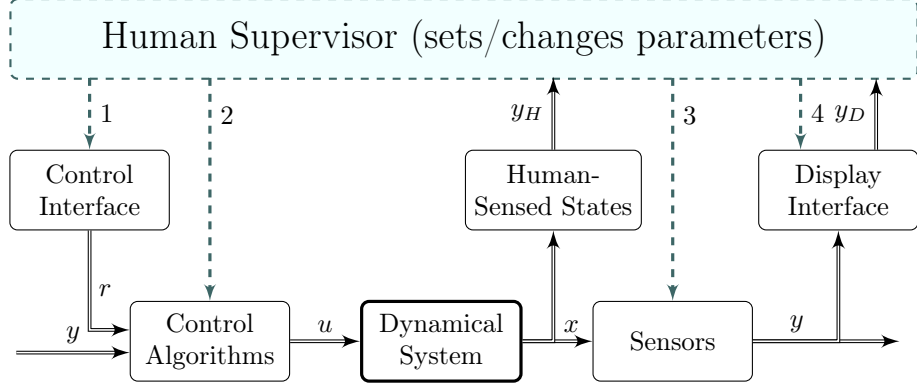


Figure 1-1: General shared decision-making and control architecture adapted from Ref. [?]

to the flight control task, is shown in Figure 1-1, where the human supervisor can modify parameters of the control interface, control law, measurements, and display interface through pathways 1-4, respectively. A division of labor similar to the one which we propose has been investigated recently in Ref. [?], where the pilot’s role is to provide an initial estimate of the anomaly severity, which is then used by an adaptive autopilot to determine a reference model and estimates of control parameters. Unlike Ref. [?], here we consider more complex anomalies which are assumed to significantly alter the plant model structure, and we explore how the pilot and autopilot can be used effectively in the anomaly response.

Anomalies in aircraft dynamical behavior can come from a number of sources, such as sensor or actuator system failures or malfunctions, changes to the inertial properties of the aircraft, structural damage, and foreign object damage [?]. As aerial vehicles increasingly depend on networked systems for guidance and navigation, there is a need to consider not only physical failures but also cyber attacks. Advanced aircraft navigation systems, which rely on the fusion of various digital sources of information to estimate the vehicle state and to guide and control the vehicle present new vulnerabilities which can have severe consequences in safety and control performance [?, ?, ?, ?]. The response to an anomaly in semi-autonomous flight is generally to transfer control to the human pilot unless the aircraft is equipped with active fault-tolerant control systems (AFTCS) that have been designed to handle the particular

type of anomaly [?]. The latter requires fault detection and diagnosis (FDD) schemes which are able to correctly and consistently detect, isolate, and diagnose anomalous and unfamiliar behavior. State of the art AFTCS which use model-based FDD are only able to retain autonomous control after anomalies which are well-defined and likely to be properly diagnosed, and for which a reconfigurable controller has been extensively verified and validated [?]. Such AFTCS, in principle, include adaptive control methods as well.

## 1.2 Contributions

In this thesis, we propose a shared decision-making and control architecture between humans and adaptive control algorithms. We consider this architecture in the context of flight control, where the desire for safety often leads to system architectures with redundancy between supervisory human operators and autonomous flight systems. We base this shared control architecture around the use of adaptive control algorithms to manage uncertainty in dynamics, and supervisory human operators who manage a shared response to anomalous changes in the structure of plant dynamics. This thesis will demonstrate and discuss how this shared decision-making and control architecture can enable overall adaptation capabilities beyond what either a human or adaptive control algorithm alone would be able to accomplish.

Chapter 2 states the problem of control of a plant in the presence of parametric uncertainties as well as sudden dynamical anomalies, which are defined in more detail. Chapter 3 presents the shared decision-making and control architecture in a simplified example, using control algorithms with a scalar input and access to the full plant state, and an onboard human pilot. Chapter 4 extends this shared decision-making and control architecture to a multi-input multi-output plant model with control design based on output feedback and remote human operators. In Chapter 5, it is shown that the resulting shared controller performs satisfactorily through extensive numerical simulation studies. Concluding remarks are given in Chapter 6.



# Chapter 2

## Problem Statement

This thesis will consider two variations in a control problem, as described in Sections 2.1 and 2.2, and addressed in Chapters 3 and 4, respectively.

### 2.1 Onboard Human Pilot and Full-State Feedback Adaptive Control

We consider single-input single-output (SISO)  $n$ th-order linear dynamical plant models of the form

$$\dot{x}_p = A_p x_p + B_p u_p, \quad y_p = C_p x_p \quad (2.1)$$

where  $x_p \in \mathbb{R}^{n \times 1}$  is a state vector, and  $A_p \in \mathbb{R}^{n \times n}$  and  $B_p \in \mathbb{R}^{n \times 1}$  are an uncertain matrix and an uncertain vector of dynamical properties, respectively, and  $u_p(t)$  is a scalar input.  $C_p \in \mathbb{R}^{1 \times n}$  is a known vector producing the scalar  $y_p$ , the plant output, which we would like to follow prescribed commands  $r(t)$  by providing a control action  $u(t)$ . For this problem, we consider the case where the vector  $x_p$ , consisting of the output  $y_p$  and its first  $n - 1$  time derivatives, is measured and available for use in feedback control, and the vector  $B_p$  is given by  $B_p = [0, \dots, 0, \beta]^T$ . We note that plants of this form have a transfer function from plant input to output given in the

Laplace frequency domain by

$$\frac{Y_p(s)}{U_p(s)} = \frac{\beta}{s^n + \alpha_{n-1}s^{n-1} + \cdots + \alpha_0} \quad (2.2)$$

where  $\alpha_i$  and  $\beta$  are arbitrary coefficients. Design of the control law  $u(t)$  is carried out under nominal conditions with the assumption

$$u_p(t) \equiv u(t). \quad (2.3)$$

Note that uncertainty in control effectiveness is captured by the uncertain matrix  $B_p$ .

In addition to an autonomous controller which generates control input  $u(t)$  in (2.3), a human operator (pilot) is tasked with the high-level operation of the plant (2.1), including monitoring to ensure safe and anomaly-free operation. Operation is thus *human-on-the-loop* as opposed to *human-in-the-loop*, as the pilot does not directly command actuator input. The pilot's perceptive capabilities (as shown in Fig. 1-1) include the sensing of  $y_D \subseteq y$ ,  $y_H$ , and  $r$ , where  $y_D$  is a subset of vehicle sensor measurements available to the pilot through cockpit displays,  $y_H$  is the human pilot's sensing through visual and vestibular modalities, and  $r$  is the prescribed command for plant output.

We consider the introduction of two severe anomalies in the dynamics of the plant model (2.1), described in Sections 2.1.1 and 2.1.2. The first consists of a change in the actuator dynamics, represented as a change in the actuator model from a gain to a first-order lag. The second anomaly is a latency introduced in the feedback of state information to the control algorithms.

The problem we investigate in Chapter 3 is whether we can use a suitable combination of

- (a) autonomous control methodologies
- (b) an onboard human pilot

to successfully mitigate the two types of anomalous dynamics to be described presently and restore tracking performance in the presence of uncertainty. We refer to this

class of anomaly response as a shared control response. This work builds on anomaly response frameworks using adaptive autopilots and on-board human pilots reported in [?] and [?].

### 2.1.1 Actuator Fault

An anomaly is introduced which changes the actuator dynamics from a direct input (2.3) to a first-order lag

$$T_L \dot{u}(t) + u(t) = u_p(t) \quad (2.4)$$

so that the dynamics of plant augmented with actuator dynamics change suddenly from order  $n$  to order  $n + 1$ . We can define an augmented plant

$$\dot{x}'_p = A'_p x'_p + B'_p u \quad (2.5)$$

where  $u(t)$  is defined in (2.4), and  $x'_p$  consists of the output  $y_p$  and its first  $n$  time derivatives. The matrix  $A'_p$  and vector  $B'_p$  are then given by

$$A'_p = \begin{bmatrix} 0 & \left[ \begin{array}{c} I_n \\ \vdots \end{array} \right] \\ \vdots & \left[ \begin{array}{c} \alpha'_0 & \dots & \alpha'_{n+1} \end{array} \right] \end{bmatrix}, \quad B'_p = \begin{bmatrix} 0 \\ \vdots \\ \beta' \end{bmatrix} \quad (2.6)$$

where  $I_n$  is the identity matrix of dimension  $n$  and  $\alpha'_i$ ,  $\beta'$  are uncertain coefficients. If the change in the order of the plant is not known to the adaptive controller, it may no longer be possible for it to stabilize the plant following such a change. The question then is if a shared decision-making architecture, with suitable action from the human pilot leading to feedback on the augmented state vector  $x'_p$ , can result in the recovery of closed-loop performance with anomalous actuator model (2.4).

### 2.1.2 Time-Delayed Sensor Measurements

We consider the introduction an anomaly in the cyber-physical space of the dynamical system with feedback control via adaptive control algorithms, which leads to latency

in the feedback of plant state information. We model this anomaly as the addition of a time delay  $\tau$  of the state measurements before the computation of the control input, causing a discrepancy between the plant state  $x_p$  and the state as sensed by the controller, denoted  $x_\sigma$ , given by

$$x_\sigma(t) = x_p(t - \tau). \quad (2.7)$$

We note that the time delay  $\tau$  may be approximated up to a certain frequency as a first-order filter, given in the Laplace frequency domain as

$$e^{-\tau s} \approx \frac{1}{1 + \tau s}. \quad (2.8)$$

In the time domain, this approximation corresponds to the differential equation

$$\tau \dot{x}_\sigma(t) + x_\sigma(t) \approx x_p(t) \quad (2.9)$$

We note that this effectively increases the order of the plant from  $n$  to  $n + 1$  when we consider the output to be the delayed signal. In this case, the augmented plant is given by

$$\dot{x}'_\sigma = A'_p x'_\sigma + B'_p u \quad (2.10)$$

with  $A'_p$  and  $B'_p$  defined in (2.6). Due to this similarity, we investigate the applicability of a shared control solution to the problem of Section 2.1.1 to the problem of a time-delayed state measurement.

## 2.2 Remote Human Operation and Output Feedback Adaptive Control

We consider the distinct problem of controlling linear multi-input multi-output (MIMO) plant models of the form

$$\begin{aligned}\dot{x}_p &= (A_p + B_p \Theta_p^T)x_p + B_p \Lambda_p u_p \\ y_p &= C_p x_p, \quad z_p = C_{pz} x_p\end{aligned}\tag{2.11}$$

where uncertain dynamics lead to the introduction of unknown  $\Theta_p$  and  $\Lambda_p$  in the plant model,  $y_p$  are measurement outputs, and  $z_p$  are regulated outputs which we would like to follow prescribed commands. It is assumed that the matrix  $CB$  has full rank, and thus the plant has uniform relative degree one (see [?]). In addition to the dynamics (2.11), the plant's actuators have the first-order dynamics

$$\dot{u}_p + (D_1 + \Theta_1^T)u_p = D_1 u \tag{2.12}$$

where  $D_1$  is a diagonal matrix representing nominal actuator parameters and  $\Theta_1$  models uncertainty in the actuator dynamics.

### 2.2.1 Actuator Fault

Consider the occurrence of an anomaly which causes a sudden change in actuator dynamics from (2.12) to the second-order model

$$\ddot{u}_p + (D_2 + \Theta_2^T)\dot{u}_p + (D_1 + \Theta_1^T)u_p = D_1 u. \tag{2.13}$$

This change in dynamics means that the the structure of the model used for control design is no longer accurate, and the autonomous controller may lose stability and command tracking ability.

In addition to an autonomous controller which generates control input  $u(t)$  in (2.12) and (2.13), a human supervisor is tasked with the high-level operation of the

plant (2.11), including mission and task planning (commanding its mode of operation) and monitoring to ensure safe and anomaly-free operation. In this paper, we consider *remote* human operators who cannot sense the vehicle state and dynamics directly through vestibular pathways. The human supervisor may be responsible for the supervision of multiple plant instances, as illustrated in Fig. 2-1 for the case of HALE VFA platforms. Operation is thus *human-on-the-loop* as opposed to *human-in-the-loop*, as the operator has no role in feedback control.

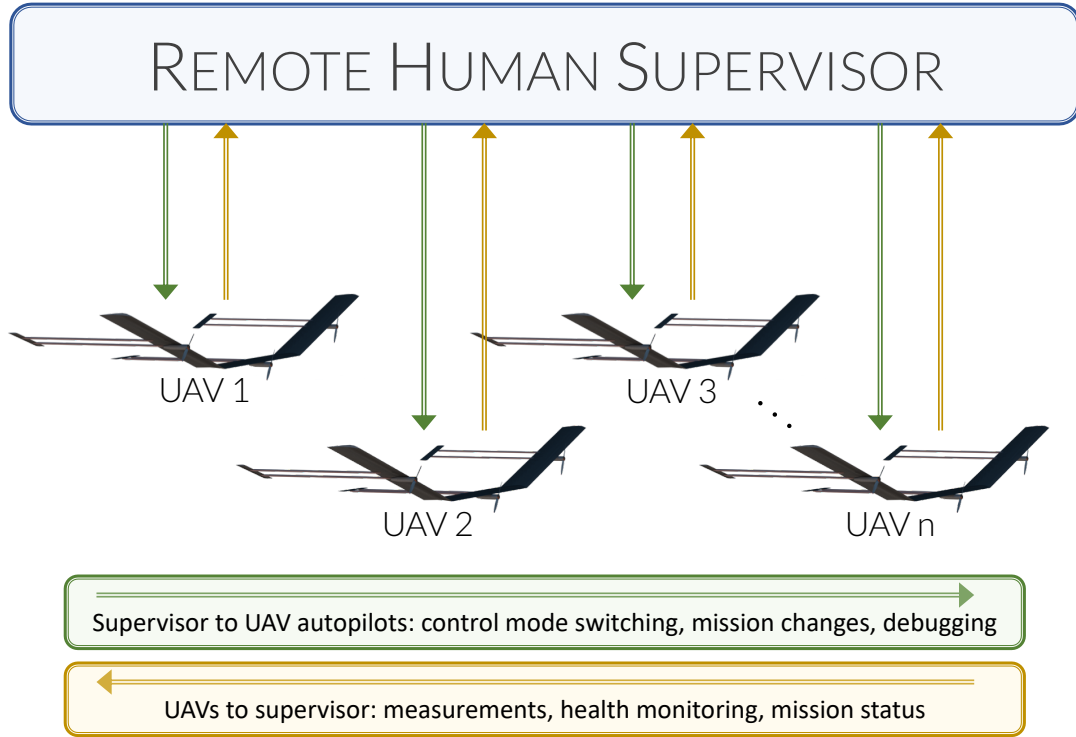


Figure 2-1: Supervisory operation of a fleet of HALE UAVs

The remote human supervisor has information on plant sensor measurements, state estimate, tracking performance, and health (via visual, haptic, and/or auditory interfaces). *Human-in-the-loop* operation is possible via remote controls, allowing the operator to actuate the plant by manually providing  $u(t)$  in (2.12) and (2.13). The sensing and actuation by the remote human supervisor include time delays  $\tau_s, \tau_a > 0$ , respectively.

The problem we investigate in Chapter 4 is whether we can use a suitable combi-

nation of

- (a) autonomous control methodologies
- (b) a remote human supervisor

to successfully mitigate the anomalous dynamics (2.13) and restore tracking performance in the presence of uncertainty.



# Chapter 3

## Shared Control with Human Pilot and State Feedback

### 3.1 The Proposed Shared Controller

As the specifics of our shared decision-making and control architecture are highly application dependent, in this chapter we will focus on the lateral-directional dynamics of a fixed-wing aircraft, which are described briefly. Chapter 4 will present the architecture in a more general form. For an aircraft trimmed in straight and level flight with equilibrium speed  $u_0$  and pitch angle  $\theta_0$ , and assuming small perturbations about the equilibrium point, the lateral-directional dynamics of the aircraft can be linearized to the form  $\dot{x}_{\text{lat}} = A_{\text{lat}}x_{\text{lat}} + B_{\text{lat}}u_{\text{lat}}$  where

$$\begin{aligned} x_{\text{lat}} &= \begin{bmatrix} \beta & p_s & \phi_s & r_s \end{bmatrix}^T, & u_{\text{lat}} &= \begin{bmatrix} \delta_r & \delta_a \end{bmatrix}^T \\ A_{\text{lat}} &= \begin{bmatrix} \frac{Y_\beta}{u_0} & \frac{Y_p}{u_0} & \frac{g_0 \cos \theta_0}{u_0} & \frac{Y_r}{u_0} - 1 \\ L_\beta & L_p & 0 & L_r \\ 0 & 1 & 0 & 0 \\ N_\beta & N_p & 0 & N_r \end{bmatrix}, & B_{\text{lat}} &= \begin{bmatrix} \frac{Y_{\delta_r}}{u_0} & \frac{Y_{\delta_a}}{u_0} \\ L_{\delta_r} & L_{\delta_a} \\ 0 & 0 \\ N_{\delta_r} & N_{\delta_a} \end{bmatrix} \end{aligned} \quad (3.1)$$

with definitions of the stability and control derivatives in matrices  $A_{\text{lat}}$  and  $B_{\text{lat}}$  skipped for brevity (see Ref. [?] for more details). The states correspond to sideslip

angle, stability axis roll rate, stability axis bank angle, and stability axis yaw rate, respectively, while the control inputs correspond to rudder and aileron deflections.

Approximate second-order linearized rolling mode dynamics are extracted from this fourth-order system, and this system is given by

$$\underbrace{\begin{bmatrix} \dot{\phi} \\ \dot{p} \end{bmatrix}}_{\dot{x}_p} = \underbrace{\begin{bmatrix} 0 & 1 \\ 0 & L_p \end{bmatrix}}_{A_p} \underbrace{\begin{bmatrix} \phi \\ p \end{bmatrix}}_{x_p} + \underbrace{\begin{bmatrix} 0 \\ L_{\delta_a} \end{bmatrix}}_{B_p} \underbrace{\delta_a}_{u_p} \quad (3.2)$$

with an open-loop transfer function

$$\frac{\Phi(s)}{\Delta_a(s)} = \frac{L_{\delta_a}}{s^2 - L_p s} \quad (3.3)$$

In these equations,  $\delta_a$  represents aileron input, and  $\phi$  and  $p$  denote the aircraft bank angle and roll rate in stability axes, with the subscript  $(\cdot)_s$  dropped for notational simplicity. It is assumed that the states  $(x_p)$  are fully available for feedback (directly from sensors for  $p$ , and via integration of  $p$  for  $\phi$ ).  $L_p$  is the roll damping derivative and  $L_{\delta_a}$  is the rolling moment due to aileron deflection. We consider scenarios in which these parameters may be unknown, but are addressed in normal operation by an MRAC-based adaptive autopilot. The system has been simplified by fixing  $\delta_r(t) = 0$  (no rudder input), so that aileron deflection is the only input. In normal operation, we assume the vehicle has sufficiently fast actuators, so that  $\delta_a(t) = u(t)$  and equivalently  $\Delta_a(s) = U(s)$ , where  $u(t)$  is the control signal.

### 3.1.1 Role of the Human Pilot

Trained human pilots develop mental models of the vehicle response and expected performance in different situations, giving these pilots a high level of situation awareness regarding the aircraft [?]. Even when a human pilot is not controlling the vehicle, anomalous vehicle behavior would be manifested through changes in the closed-loop response of the vehicle and its disturbance-rejection abilities. When the cockpit controls used in manual control are physically actuated during autopilot operation, the

pilot may be able perceive the autopilot's control actions through kinesthetic or tactile feedback [?, ?]. In combination with the pilot's visual and vestibular sensing of vehicle dynamics, this sensing of autopilot control actions will allow the human pilot to determine the open-loop vehicle response and perceive anomalous behavior. We therefore hypothesize that an on-board human pilot has the sensory and perceptive capabilities to detect and diagnose anomalies such as those described above.

Our assumptions are that the human pilot can sense (i)  $y_D \subseteq y$ , (ii)  $r$ , (iii)  $u$ , (iv)  $\delta_a$ , and (v)  $y_H$ , where  $y_D$  is a subset of vehicle sensor measurements available to the pilot, and  $y_H$  is the human pilot's sensing independent of the vehicle's sensors. The hypothesis is that (i)-(iii) are accessible through cockpit displays, (iv) is accessible through cockpit control interfaces, and (v) is accessible through the pilot's visual and vestibular sensing. In addition to changes in closed-loop behavior in both anomalies introduced in Section 2, the physical actuator fault would change the relationship between  $u$  and  $\delta_a$ , while the time-delayed sensor measurements would change the relationship between  $y_H$  and  $y_D$ , in addition to the closed-loop vehicle dynamics. We hypothesize that incorporating the human pilot in detection and decision-making tasks may allow the autopilot to retain autonomous control in situations where reliance on autonomous anomaly detection and diagnosis is impractical.

### 3.1.2 MRAC-Based Adaptive Autopilot

Central to this work is the use of an autopilot which employs advanced control principles for low-level flight control tasks in the place of human pilots. In particular, our autopilot design uses MRAC, with vehicle states available for feedback [?]. Closed-loop reference models (CRMs) based on Ref. [?] are utilized here to improve the transient performance of MRAC, in comparison to open-loop reference models.

The plant to be controlled is an  $n$ th-order linear dynamical system given in (2.1). We design a feedforward/feedback control law of the form

$$u(t) = \theta(t)x_p(t) + q(t)r(t) \quad (3.4)$$

where  $\theta(t) \in \mathbb{R}^{1 \times n}$  and scalar  $q(t)$  are adaptive gains on the plant states and reference input,  $r(t)$ , respectively.

The reference model used in this adaptive controller is a dynamical system

$$\dot{x}_m(t) = A_m x_m(t) + B_m r(t) - L_m [x_p(t) - x_m(t)] \quad (3.5)$$

where  $A_m \in \mathbb{R}^{n \times n}$  is Hurwitz,  $B_m \in \mathbb{R}^{n \times 1}$ ,  $L_m \in \mathbb{R}^{n \times n}$ , and  $e(t) \equiv x_p(t) - x_m(t)$  defined as the state error. It is assumed that there exists scalar  $\lambda$  such that  $B_p \equiv \lambda B_m$ . In this form, an appropriate choice of  $L_m$ , such as (3.8), ensures that there exists matrix  $P = P^T > 0$ , the solution to the Lyapunov equation  $(A_m + L_m)^T P + P(A_m + L_m) = -Q$ , for arbitrary  $Q = Q^T > 0$ . Feedback and feedforward control gain adaptation is given by

$$\dot{\theta}(t) = -\Gamma_\theta B_m^T P e(t) x_p^T(t) \quad (3.6)$$

$$\dot{q}(t) = -\gamma_q B_m^T P e(t) r(t) \quad (3.7)$$

where  $\Gamma_\theta > 0$  and  $\gamma_q > 0$  are a diagonal matrix and scalar, respectively, of constant weights. These weights correspond to learning rates on the feedback/feedforward parameters. The state error feedback gain,  $L_m$ , can be chosen to be

$$L_m = -A_m - \Gamma_\theta \quad (3.8)$$

which ensures stability of the closed-loop reference model dynamics. With the plant, control law, and reference model dynamics defined in (??), (3.4), and (3.5), respectively, the equations defining the feedback and feedforward gains  $\theta^*$  and  $q^*$  which match the dynamics of the closed-loop system to that of the reference model exactly are

$$A_p + B_p \theta^* = A_m \quad (3.9)$$

$$B_p q^* = B_m \quad (3.10)$$

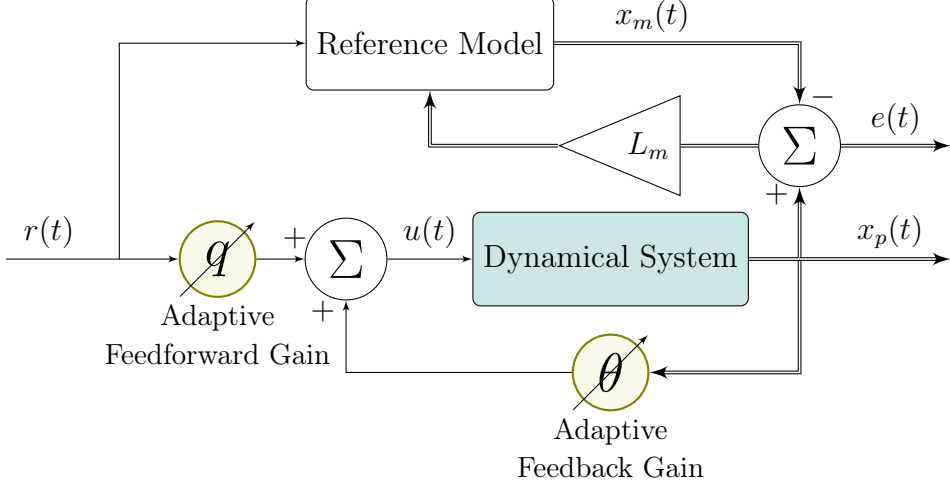


Figure 3-1: Block diagram of model-reference adaptive controller with closed-loop reference model

To ensure robustness of the adaptive controller, a projection operator[?, ?] is used in conjunction with the adaptive laws (3.6) and (3.7). The projection operator limits the magnitude of  $\dot{\theta}(t)$  and  $\dot{q}(t)$ , so that the parameters  $\theta(t)$  and  $q(t)$  remain within a convex set. The reader is referred to Ref. [?] for a detailed treatment of the projection operator as it applies to the general CRM-adaptive controller, but to summarize, the adaptive laws are modified from (3.6) and (3.7) to be

$$\dot{\theta}(t) = \text{Proj}(-\Gamma_\theta B_m^T P e(t) x_p^T(t), \theta(t)) \quad (3.11)$$

$$\dot{q}(t) = \text{Proj}(-\gamma_q B_m^T P e(t) r(t), q(t)) \quad (3.12)$$

with the vector projection operator defined as

$$\text{Proj}(Y, \Phi) = [\text{Proj}(y_1, \varphi_1) \dots \text{Proj}(y_n, \varphi_n)] \quad (3.13)$$

and the scalar projection operator defined as

$$\text{Proj}(y, \varphi) = \begin{cases} y(1 - f(\varphi)) & f(\varphi) > 0 \wedge y \nabla f(\varphi) > 0 \\ y & \text{otherwise} \end{cases} \quad (3.14)$$

The function  $f(\varphi)$  is taken to be

$$f(\varphi) = \frac{\varphi^2 - \varphi_m^2}{2\varphi_\epsilon\varphi_m + \varphi_\epsilon^2} \quad (3.15)$$

where  $\varphi_m$  and  $(\varphi_m + \varphi_\epsilon)$  define “soft” and “hard” bounds on the parameter  $\varphi$ , respectively.

Under nominal vehicle operation with the plant given by (3.2), a second-order reference model corresponding to (3.5) is used

$$\underbrace{\begin{bmatrix} \dot{\phi}_d \\ \dot{p}_d \end{bmatrix}}_{\dot{x}_m} = \underbrace{\begin{bmatrix} 0 & 1 \\ -a_{m,1} & -a_{m,2} \end{bmatrix}}_{A_m} \underbrace{\begin{bmatrix} \phi_d \\ p_d \end{bmatrix}}_{x_m} + \underbrace{\begin{bmatrix} 0 \\ b_{m,2} \end{bmatrix}}_{B_m} r(t) - L_m e(t) \quad (3.16)$$

where  $x_m(t)$  is a vector of the desired states and  $r(t)$  is the commanded bank angle.

It is straightforward to see that a choice of

$$\theta^* = \begin{bmatrix} -a_{m,1} \\ L_{\delta_a} \end{bmatrix} \quad (3.17)$$

$$q^* = \frac{b_{m,2}}{L_{\delta_a}} \quad (3.18)$$

solves the matching condition in (3.9) and (3.10). This in turn implies that even if the roll damping derivative ( $L_p$ ) and the rolling moment due to aileron deflection ( $L_{\delta_a}$ ) are unknown, the adaptive controller in (3.4), (3.11), and (3.12) will be able to vary the feedback and feedforward gains such that the closed-loop response of the system is satisfactory. We shall denote such a case as nominal operation, and consider the anomalous cases as those where in addition to parametric uncertainties, changes in dynamics as denoted in cases (i) and (ii) above occur.

### 3.1.3 The Overall Shared Controller

The shared control algorithm between the adaptive autopilot and human pilot that we propose is as follows. At time  $t = 0$ , the adaptive controller as in (3.4), (3.11), and (3.12) is proposed, where the state  $x_p$  is given as in (3.2). An anomaly either as

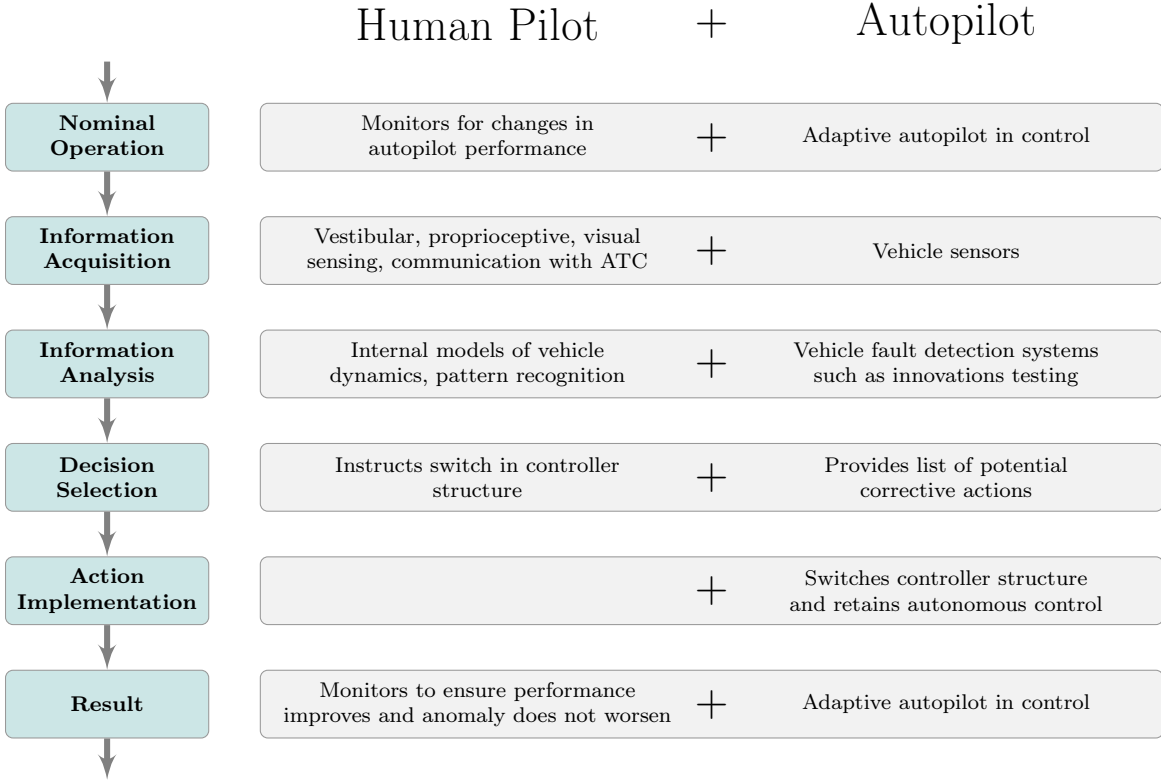


Figure 3-2: Our proposal for shared decision making following an anomaly, with stages of decision making categorized in Ref. [?]

in case (i) or case (ii) is assumed to occur at  $t = t_{s,p}$ .

Following this time instant, the pilot detects the anomalous vehicle dynamics, and at  $t = t_{s,c}$  indicates to the adaptive autopilot the perceived increase in order. Using this pilot input, we propose an adaptive controller predicated on a third-order dynamics of the open-loop plant and assume that in addition to the bank angle and roll rate, angular acceleration  $\dot{p}$  is also measurable. We choose a reference model as

$$\underbrace{\begin{bmatrix} \dot{\phi}_d \\ \dot{p}_d \\ \ddot{p}_d \end{bmatrix}}_{\dot{x}'_m} = \underbrace{\begin{bmatrix} 0 & 1 & 0 \\ 0 & 0 & 1 \\ -a'_{m,1} & -a'_{m,2} & -a'_{m,3} \end{bmatrix}}_{A'_m} \underbrace{\begin{bmatrix} \phi_d \\ p_d \\ \dot{p}_d \end{bmatrix}}_{x'_m} + \underbrace{\begin{bmatrix} 0 \\ 0 \\ b'_{m,3} \end{bmatrix}}_{B'_m} r - L'_m e' \quad (3.19)$$

The time interval  $[t_{s,p}, t_{s,c}]$  is indicated as Post-Anomaly and the interval  $t \geq t_{s,c}$  is indicated as Post-Correction. For case (i),  $\theta^* \in \mathbb{R}^3$  and  $q^*$  exist that solve the

corresponding matching conditions in (3.9) and (3.10), and an adaptive controller as in (3.11) and (3.12) can be realized to lead to a stable closed-loop solutions and accurate tracking. These matching conditions are not met, however, in case (ii). In the numerical examples, we will discuss the details of how such an adaptive controller with an increase in dimension following the pilot input performs for both cases of anomalies.

A detailed discussion of the stability of the resulting adaptive controller is not carried out in this thesis. But it is clear that if the Post-Anomaly phase is sufficiently short, the adaptive controller will guarantee boundedness of the closed-loop system and convergence of  $e(t)$  to zero if our assumptions that the cause of the two anomalies results in a third-order plant and that its states are measurable are satisfied. We carry out a detailed simulation study in the following section and evaluate the performance of the shared controller proposed above.

# Chapter 4

## Shared Control with Remote Human Pilot and Output Feedback

We introduce a shared decision-making and control framework with the goal of enabling the safe operation of HALE UAVs subject to both parametric uncertainties and the sudden introduction of anomalous, unmodeled dynamics as described in the preceding section. The shared control framework is based on a combination of actions by UAV autopilots and remote human operators. MRAC autopilots and complementary higher-level motion planning algorithms allow for continuous autonomous operation of the UAVs under nominal conditions. Remote human operators monitor the performance of the vehicles and are trained and able to remotely pilot the vehicle in case of autopilot failure. The remote piloting of the vehicles, however, is a daunting task due to communication delays and a weakened understanding of the vehicle dynamics, state, and environment, due to the remote nature of the task. Our shared anomaly response involves the remote human operator to diagnose and correct for the dynamical anomaly without taking over manual control of the vehicle. In Section 4.1, we describe two adaptive autopilot designs which in combination with the human operator whose precise role is described subsequently in Section 4.2, will solve the problem presented in Section 2.

## 4.1 Adaptive Output-Feedback Control

An autonomous controller is designed to track prescribed commands for plant outputs  $z_p(t)$  in (2.11). The shared control framework involves separate MRAC designs for the plant (2.11) in combination with actuator dynamics (2.12) and (2.13). The control design accommodating first-order actuators is denoted the “nominal” control design, and excluding exceptional failures, is the controller in use by the UAV autopilot. The control design accommodating second-order actuators is a predefined “recovery” controller, whose use case will be defined more fully in Section 4.2. To achieve the control goals stated in Section 2, control design consists of

- (i) baseline control design using the robust servomechanism linear quadratic regulator method (RSLQR);
- (ii) adaptive output-feedback augmentation for parametric uncertainties in the plant.

Control design in each case uses an augmented linear plant formulation, where the plant (2.11) is extended with the actuator dynamics – either (2.12) or (2.13) – as well as integrated tracking errors

$$e_z^T(t) = \int_0^t (z_p(\tau) - z_{cmd}(\tau)) d\tau. \quad (4.1)$$

The augmented plant model with  $x = [x_p^T \ x_{act}^T \ (e_z^T)^T]^T$  can be written compactly as

$$\begin{aligned} \dot{x} &= (A + B_1 \Psi_1^T + B_r \Psi_r^T) x + B_r \Lambda u + B_z z_{cmd} \\ y &= Cx, \quad z = C_z x \end{aligned} \quad (4.2)$$

where  $x \in \mathbb{R}^n$ ,  $u \in \mathbb{R}^m$ ,  $y \in \mathbb{R}^p$  are redefined states, inputs and outputs, respectively. This plant contains unknown matrices  $\Psi_1$ ,  $\Psi_r$ , and  $\Lambda$ , which hold the state-dependent plant uncertainties, state-dependent actuator dependencies, and actuator effectiveness, respectively. The exact forms of  $B_r$  and  $\Psi_r$  depend on whether the actuators are first-order (2.12) or second-order (2.13), and the subscript  $r$  indicates the relative degree of the augmented plant. It is noted that the augmented plant model which

arises from the inclusion of actuator model (2.12) in the plant (2.11) has relative degree two, while the augmented plant model associated with the inclusion of actuator model (2.13) has relative degree three.

For control design, closed-loop reference models ([?]) are designed as

$$\dot{x}_m = A_m x_m + B_z z_{cmd} + L e_y + \mathcal{F}_r(t), \quad y_m = C x_m \quad (4.3)$$

where  $e_y = y - y_m$ ,  $A_m = A - B_r K^T$  with  $K \in \mathbb{R}^{n \times m}$  is a baseline feedback control gain designed for the system without uncertainty using RSLQR, as described by [?].  $L$  is a Luenberger-like feedback gain, and  $\mathcal{F}_r(t)$  is a function used when  $r \geq 2$  to recover stability properties in the presence of uncertainty.

In what follows, control designs for the “nominal” controller and for the “recovery” controller are summarized, assuming (for simplicity, but without loss of generality) that the augmented plant model (4.2) is square (i.e.  $m = p$ ). Readers are referred to [?] and [?] for a more thorough treatment of the adaptive control designs in this article.

#### 4.1.1 Nominal Adaptive Control Design

The control design for the plant with first-order actuator dynamics summarized by giving definitions for CRM residual gain matrix  $L$ , function  $\mathcal{F}_2(t)$ , control law  $u(t)$ , and parameter adaptation. Note that  $B_2$  represents  $B_r$  from (4.2) for this relative degree two plant.

The feedback matrix  $L$  is designed as follows. We define the “relative degree one input path”

$$B_1^a = \alpha_0 B_2 + \alpha_1 A B_2 \quad (4.4)$$

where  $\alpha_i > 0$  are free design parameters. We then define

$$S = (CB_1^a)^T \quad (4.5)$$

$$\bar{C} = SC \quad (4.6)$$

$$R^{-1} = (\bar{C}B_1^a)^{-1} [\bar{C}AB_1^a + (\bar{C}AB_1^a)^T] (\bar{C}B_1^a)^{-1} + \epsilon I \quad (4.7)$$

$$L = B_1^a R^{-1} S \quad (4.8)$$

where  $\epsilon > 0$  [?, Eq. 30] is chosen to guarantee stability of the adaptive system.

The function  $\mathcal{F}_2(t)$  makes use of scaled error signal

$$e_{sy}(t) = R^{-1} S e_y(t) \quad (4.9)$$

and a filtered version of this signal,  $\bar{e}_{sy}(t)$ , given in the form of a differential equation as

$$(\alpha_0 + \alpha_1 \frac{d}{dt}) \{\bar{e}_{sy}(t)\} = \alpha_1 e_{sy}(t). \quad (4.10)$$

It is worth noting that this can be represented in the Laplace  $s$ -domain as

$$\bar{E}_{sy}(s) = \frac{\alpha_1}{\alpha_1 s + \alpha_0} E_{sy}(s).$$

$\mathcal{F}_2(t)$  is then defined as

$$\mathcal{F}_2(t) = B_2 (\alpha_0 + \alpha_1 \frac{d}{dt}) \{\hat{\Psi}_m^T(t) \bar{e}_{sy}(t)\} \quad (4.11)$$

where  $\hat{\Psi}_m(t)$  is a matrix of adaptive parameters. Similar to (4.10), we define filtered reference model state,  $\bar{x}_m(t)$ , with the differential equation

$$(\alpha_0 + \alpha_1 \frac{d}{dt}) \{\bar{x}_m(t)\} = \alpha_1 x_m(t). \quad (4.12)$$

We define a regressor vector of known signals as

$$\mathcal{X}(t) = [(K^T \bar{x}_m)^T, \quad x_m^T, \quad \bar{x}_m^T]^T. \quad (4.13)$$

The control law,  $u(t)$ , is then given by

$$u(t) = -(\alpha_0 + \alpha_1 \frac{d}{dt}) \{\hat{\Psi}_\Lambda^T(t) \mathcal{X}(t)\} \quad (4.14)$$

where  $\hat{\Psi}_\Lambda(t)$  is a matrix of adaptive parameters. The laws for adaptation of parameter matrices  $\hat{\Psi}_m(t)$  and  $\hat{\Psi}_\Lambda(t)$  are given by

$$\begin{aligned} \dot{\hat{\Psi}}_m(t) &= \Gamma_m \bar{e}_{sy}(t) e_y^T(t) S^T \\ \dot{\hat{\Psi}}_\Lambda(t) &= -\Gamma_\Lambda \mathcal{X}(t) e_y^T(t) S^T \end{aligned} \quad (4.15)$$

with diagonal adaptation gains  $\Gamma_m$ ,  $\Gamma_\Lambda > 0$ . We note that the derivatives of the adaptive parameters, computed in (4.15), are used to implement (4.11) and (4.14) with the product rule of differentiation.

#### 4.1.2 Recovery Adaptive Control Design

Control design with the second-order actuator model is similar to that described above, but requires modifications to ensure strict positive realness of the transfer matrix of the model-following error dynamics.

The definition of  $L$  is modified by replacing  $B_1^a$  in (4.4) with

$$B_1^a = \alpha_0 B_3 + \alpha_1 A B_3 + \alpha_2 A^2 B_3 \quad (4.16)$$

and proceeding with (4.5)–(4.8). A definition for  $\epsilon > 0$  in this case can be found in [?]. To simplify notation, the operator  $\Pi\{\cdot\}$  is defined as

$$\Pi\{\cdot\} = (\alpha_0 + \alpha_1 \frac{d}{dt} + \alpha_2 \frac{d^2}{dt^2})\{\cdot\}. \quad (4.17)$$

The function  $\mathcal{F}_3(t)$  utilizes filtered error vectors  $\bar{e}_{sy}^{[1]}(t)$ ,  $\bar{e}_{sy}^{[2]}(t)$ , and  $\bar{e}_{sy}^{[1][2]}(t)$ , defined

by the differential equations

$$\begin{aligned}\Pi\{\bar{e}_{sy}^{[1]}(t)\} &= (\alpha_1 + \alpha_2 \frac{d}{dt})\{e_{sy}(t)\} \\ \Pi\{\bar{e}_{sy}^{[2]}(t)\} &= \alpha_2 e_{sy}(t) \\ \Pi\{\bar{e}_{sy}^{[1][2]}(t)\} &= (\alpha_2 \frac{d}{dt})\{\hat{\phi}_1^T(t)\bar{e}_{sy}^{[1]}(t)\}\end{aligned}\tag{4.18}$$

where  $e_{sy}(t)$  was defined in (4.9),  $\hat{\phi}_1(t)$  is a vector of adaptive parameters, and coefficients  $\alpha_i > 0$  are free design parameters. We define the integrated and scaled measurement output error,

$$e_y^{\mathcal{I}}(t) = \int_0^t L(y(\tau) - y_m(\tau)) d\tau\tag{4.19}$$

which is used to define filtered error signals  $\bar{e}_{\mathcal{I}y}^{[1]}(t)$  and  $\bar{e}_{\mathcal{I}y}^{[1][2]}(t)$ , given by

$$\begin{aligned}\Pi\{\bar{e}_{\mathcal{I}y}^{[1]}(t)\} &= (\alpha_1 \frac{d}{dt} + \alpha_2 \frac{d^2}{dt^2})\{\hat{\Phi}_1^T(t)e_y^{\mathcal{I}}(t)\} \\ \Pi\{\bar{e}_{\mathcal{I}y}^{[1][2]}(t)\} &= (\alpha_2 \frac{d}{dt})\{\hat{\Lambda}(t)\bar{e}_{\mathcal{I}y}^{[1]}(t)\}\end{aligned}\tag{4.20}$$

where  $\hat{\Phi}_1(t)$  and  $\hat{\Lambda}(t)$  are matrices of adaptive parameters. We define operators

$$\begin{aligned}f_a\{\cdot\} &= (\alpha_0 \alpha_2 B_3 + (\alpha_1 B_3 + \alpha_2 A B_3) \frac{d}{dt})\{\cdot\} \\ f_b\{\cdot\} &= \alpha_2 B_3 \Pi\{\cdot\}\end{aligned}\tag{4.21}$$

and use these to define

$$\begin{aligned}\mathcal{F}_3(t) &= f_a\{\hat{\phi}_1^T(t)\bar{e}_{sy}^{[1]}(t) - \hat{\Lambda}^T(t)\bar{e}_{\mathcal{I}y}^{[1]}(t)\} \\ &\quad + f_b\{\hat{\phi}_1^T(t)[\bar{e}_{sy}^{[1][2]}(t) - \bar{e}_{\mathcal{I}y}^{[1][2]}(t)] + \hat{\phi}_2^T(t)\bar{e}_{sy}^{[2]}(t)\}\end{aligned}\tag{4.22}$$

where  $\hat{\phi}_2(t)$  is an additional vector of adaptive parameters.

We define filtered reference model states  $\bar{x}_m^{[1]}$  and  $\bar{x}_m^{[2]}$  as

$$\begin{aligned}\Pi\{\bar{x}_m^{[1]}(t)\} &= (\alpha_1 + \alpha_2 \frac{d}{dt})\{x_m(t)\} \\ \Pi\{\bar{x}_m^{[2]}(t)\} &= \alpha_2 x_m(t).\end{aligned}\tag{4.23}$$

Variable  $\bar{v}_m(t)$  is introduced, with artificial time derivatives, such that

$$\begin{aligned}\bar{v}_m &= x_m, \quad \frac{d}{dt}\{\bar{v}_m\} = Ax_m + B_z z_{cmd} \\ \frac{d^2}{dt^2}\{\bar{v}_m\} &= A^2 x_m + AB_z z_{cmd} + B_z \frac{dz_{cmd}}{dt} - ALe_y.\end{aligned}\tag{4.24}$$

The regressor vector  $\mathcal{X}(t)$  is redefined as

$$\mathcal{X}(t) = [(K^T \bar{x}_m^{[2]})^T, \quad \bar{v}_m^T, \quad \bar{x}_m^{[1]T}, \quad \bar{x}_m^{[2]T}]^T.\tag{4.25}$$

The control law  $u(t)$  for the “recovery” controller is

$$\begin{aligned}u(t) &= -\Pi\{\hat{\Psi}^T(t)\mathcal{X}(t)\} \\ &\quad -(\alpha_1 \frac{d}{dt} + \alpha_2 \frac{d^2}{dt^2})\{\hat{\Phi}_1^T(t)\}e_y^T(t)\end{aligned}\tag{4.26}$$

where

$$\hat{\Psi}(t) = [\hat{\Upsilon}^T(t), \quad \hat{\Phi}_1^T(t), \quad \hat{\Phi}_2^T(t), \quad \hat{\Phi}_3^T(t)]^T\tag{4.27}$$

is a matrix of adaptive parameters.

In this controller, the laws for parameter adaptation use second-order tuners as in [?]. We first define a regressor vector  $\nu(t)$  of filtered error signals

$$\nu(t) = \left[(\bar{e}_{\mathcal{I}y}^{[1][2]} - \bar{e}_{sy}^{[1]} - \bar{e}_{sy}^{[1][2]})^T, \quad (-\bar{e}_{sy}^{[2]})^T, \quad (\bar{e}_{\mathcal{I}y}^{[1]})^T\right]^T\tag{4.28}$$

and associated matrix of adaptive parameters

$$\hat{\Theta}(t) = [\hat{\phi}_1^T(t), \quad \hat{\phi}_2^T(t), \quad \hat{\Lambda}^T(t)].\tag{4.29}$$

Inputs to the second-order tuners are calculated by integrating

$$\begin{aligned}\dot{\hat{\Psi}}'(t) &= \Gamma_\Psi \mathcal{X} e_y^T S^T \text{sgn}(\Lambda) \\ \dot{\hat{\Theta}}'(t) &= -\Gamma_\Theta \nu e_y^T S^T\end{aligned}\tag{4.30}$$

where  $\Gamma_\Psi, \Gamma_\Theta > 0$  are diagonal adaptation gains.

The desired matrices of adaptive parameters are outputs of the tuners

$$\begin{aligned}\dot{X}_{\hat{\Psi}}(t) &= (A_T X_{\hat{\Psi}} + B_T (\hat{\Psi}'(t))^T) g(\mathcal{X}, \mu_{\mathcal{X}}) \\ \hat{\Psi}(t) &= (C_T X_{\hat{\Psi}})^T \\ \dot{X}_{\hat{\Theta}}(t) &= (A_T X_{\hat{\Theta}} + B_T (\hat{\Theta}'(t))^T) g(\nu, \mu_{\nu}) \\ \hat{\Theta}(t) &= (C_T X_{\hat{\Theta}})^T\end{aligned}\tag{4.31}$$

where

$$g(\mathbf{x}, \mu) = 1 + \mu \mathbf{x}^T \mathbf{x}\tag{4.32}$$

is a time-varying gain with scalar gain  $\mu$  described in [?].  $A_T \in \mathbb{R}^{2m \times 2m}$ ,  $B_T \in \mathbb{R}^{2m \times m}$ , and  $C_T \in \mathbb{R}^{m \times 2m}$  are block diagonal matrices with diagonal blocks

$$A_{T,i} = \begin{bmatrix} 0 & 1 \\ -\frac{\alpha_0}{\alpha_2} & -\frac{\alpha_1}{\alpha_2} \end{bmatrix}, \quad B_{T,i} = \begin{bmatrix} 0 \\ \frac{\alpha_0}{\alpha_2} \end{bmatrix}, \quad C_{T,i} = \begin{bmatrix} 1 & 0 \end{bmatrix}\tag{4.33}$$

Derivatives of the adaptive parameters, used in (4.18), (4.20), (4.22), and (4.26), are given by

$$\begin{aligned}\dot{\hat{\Psi}}(t) &= (C_T^\delta X_{\hat{\Psi}})^T, & \ddot{\hat{\Psi}}(t) &= (C_T^{\delta\delta} X_{\hat{\Psi}})^T \\ \dot{\hat{\Theta}}(t) &= (C_T^\delta X_{\hat{\Theta}})^T, & \ddot{\hat{\Theta}}(t) &= (C_T^{\delta\delta} X_{\hat{\Theta}})^T\end{aligned}\tag{4.34}$$

where  $C_T^\delta, C_T^{\delta\delta} \in \mathbb{R}^{m \times 2m}$  are block diagonal matrices with diagonals  $C_{T,i}^\delta = [0, 1]$  and  $C_{T,i}^{\delta\delta} = -\frac{1}{\alpha_2} [\alpha_0, \alpha_1]$ .

## 4.2 Human Supervisor

We task the remote human supervisor with the following three responsibilities for shared anomaly response on the HALE VFA platform.

1. Timely detection and characterization of anomalous closed-loop dynamical behavior
2. Isolation of control loop with anomalous behavior (i.e. longitudinal or lateral-directional)
3. Commanding a change from nominal autopilot (4.4)–(4.15) to recovery autopilot (4.16)–(4.34)

The first task requires an attentive human operator able to discern that

- (a) an anomaly has occurred and control performance degradation is not caused solely by external disturbances;
- (b) swift action must be taken in order to recover stability and performance;
- (c) it may be possible to recover stability and performance via corrective action.

The second task requires a human operator with knowledge and familiarity with the VFA dynamics and control structure to understand which control loop (e.g. pitch mode, roll mode, airspeed) is the source of the anomalous dynamics.

The final task for the trained remote human operator is the transfer of this diagnosis to the autopilot, by changing the relevant controller to its “recovery” mode.

Note that while the remote human operator is assumed to have the training and controls necessary to disable all autopilot functionality and control the vehicle manually, this shared anomaly response deliberately circumvents any *human-in-the-loop* (manual) control.



# Chapter 5

## Anomaly Response Simulations

### 5.1 State Feedback

The two cases discussed above, of the introduction of actuator dynamics and a time delay, respectively, were simulated numerically in MATLAB/Simulink for bank angle tracking tasks. In these simulations, the commanded stability axis bank angle is a sequence of 5-second steps. In both of the examples presented here, the anomaly occurs at  $t_{s,p} = 30\text{s}$ , and the corrective action is applied to the controller at  $t_{s,c} = 90\text{s}$ .

Numerical data for the Boeing 747 flying straight-and-level at Mach 0.25 at sea level[?] was substituted into (3.2) to constitute the following nominal plant dynamics, beginning at time  $t = 0$

$$\dot{x}_p = \begin{bmatrix} 0 & 1 \\ 0 & -1.10 \end{bmatrix} x_p + \begin{bmatrix} 0 \\ 0.318 \end{bmatrix} \delta_a \quad (5.1)$$

which resulted in the open-loop transfer function

$$\frac{\Phi(s)}{\Delta_a(s)} = \frac{0.318}{s^2 + 1.10s} \quad (5.2)$$

A reference model was chosen as in (3.16) given by

$$\dot{x}_m = \underbrace{\begin{bmatrix} 0 & 1 \\ -8 & -6 \end{bmatrix}}_{A_m} x_m + \underbrace{\begin{bmatrix} 0 \\ 8 \end{bmatrix}}_{B_m} r - \underbrace{\begin{bmatrix} -10 & -1 \\ 8 & -4 \end{bmatrix}}_{L_m} e \quad (5.3)$$

for the first (“nominal” and “post-anomaly”) stages of simulation. The initial feedback and feedforward parameters  $\theta(t = 0)$  and  $q(t = 0)$  are chosen such that the matching conditions of (3.17) and (3.18) are met.

### 5.1.1 Actuator Fault

By applying the change in dynamics defined in (2.4), and choosing  $T_l = 0.556$ , the plant dynamics in (2.6) become

$$\dot{x}'_p = \begin{bmatrix} 0 & 1 & 0 \\ 0 & 0 & 1 \\ 0 & -1.98 & -2.90 \end{bmatrix} x'_p + \begin{bmatrix} 0 \\ 0 \\ 0.5724 \end{bmatrix} u \quad (5.4)$$

at  $t = t_{s,p}$ , resulting in the open-loop transfer function

$$\frac{\Phi(s)}{U(s)} = \frac{0.5724}{s^3 + 2.90s^2 + 1.98s} \quad (5.5)$$

After detection and diagnosis of the anomaly with the shared decision-making framework, the corrective action to increase the dimension of the controller is made at  $t = t_{s,c}$ , and the reference model dynamics (with a pole added to the second-order reference model at  $s = -4$ ) becomes that of (3.19) given by

$$\dot{x}'_m = \underbrace{\begin{bmatrix} 0 & 1 & 0 \\ 0 & 0 & 1 \\ -32 & -32 & -10 \end{bmatrix}}_{A'_m} x'_m + \underbrace{\begin{bmatrix} 0 \\ 0 \\ 32 \end{bmatrix}}_{B'_m} r - \underbrace{\begin{bmatrix} -10 & -1 & 0 \\ 0 & -10 & -1 \\ 32 & 32 & 0 \end{bmatrix}}_{L'_m} e' \quad (5.6)$$

The feedback (and corresponding feedforward) gains which will cause the closed-loop roll response to match the desired response exactly are

$$\theta^*(t) = \begin{cases} \begin{bmatrix} -25.16, & -15.41 \\ -55.91, & -52.45, & -5.07 \end{bmatrix} & t < t_{s,p} \\ \begin{bmatrix} 25.16 & & \\ & 55.91 & \end{bmatrix} & t \geq t_{s,p} \end{cases} \quad (5.7)$$

$$q^*(t) = \begin{cases} 25.16 & t < t_{s,p} \\ 55.91 & t \geq t_{s,p} \end{cases} \quad (5.8)$$

which are unknown to the adaptive controller. As mentioned earlier, we chose  $\theta(t = 0) = [-25.16, -15.41]$  and  $q(t = 0) = 25.16$ . The learning rates in (3.11) and (3.12) were chosen to be  $\Gamma_\theta = 10I_2$ , with  $I_n$  the identity matrix of dimension  $n$ , and  $\gamma_q = 10$ . The projection operator was not used in this simulation. It was assumed that  $t_{s,p} = 30$ s and  $t_{s,c} = 90$ s. To add more realism to the simulation example, we have assumed that the signal  $\dot{p}$  is not directly measured, and instead use a high-pass filter to estimate it from  $p$  using  $\hat{p} = \frac{as}{s+a}p$ . Results of this simulation are given in Figures 5-1, 5-2, 5-3, and 5-4.

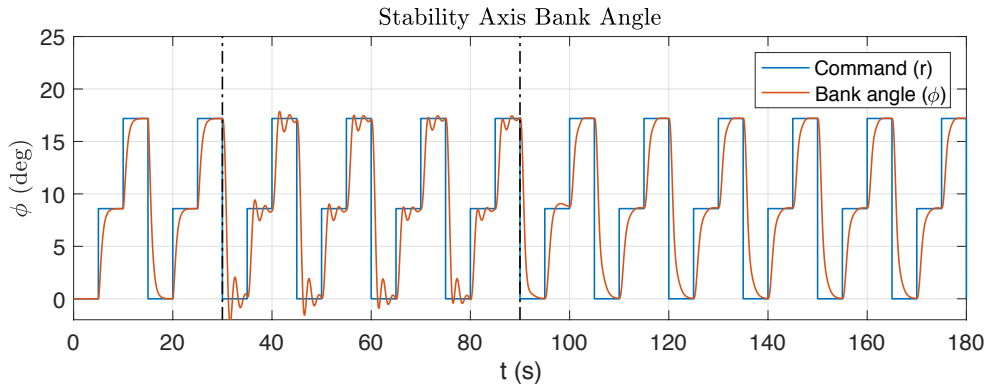


Figure 5-1: Command ( $r$ ) and output ( $\phi$ ): under nominal operation ( $t \leq 30$  s), after the change in actuator dynamics ( $30 < t \leq 90$  s), and after a corrective action to switch the controller ( $t > 90$  s)

From Figures 5-1, 5-2, and 5-3, it is clear that after an initial adaptation period, the adaptive controller with third-order reference model dynamics converges on the desired feedback/feedforward gains, returning the roll control to its satisfactory per-

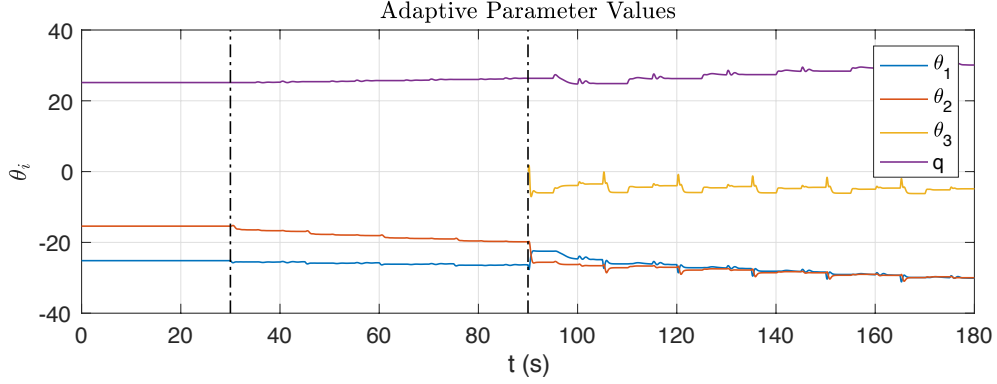


Figure 5-2: Adaptive feedback gains for the same simulation example as in Figure 5-1: under nominal operation ( $t \leq 30$  s), after the change in actuator dynamics ( $30 \text{ s} < t \leq 90$  s), and after a corrective action to switch the controller ( $t > 90$  s)

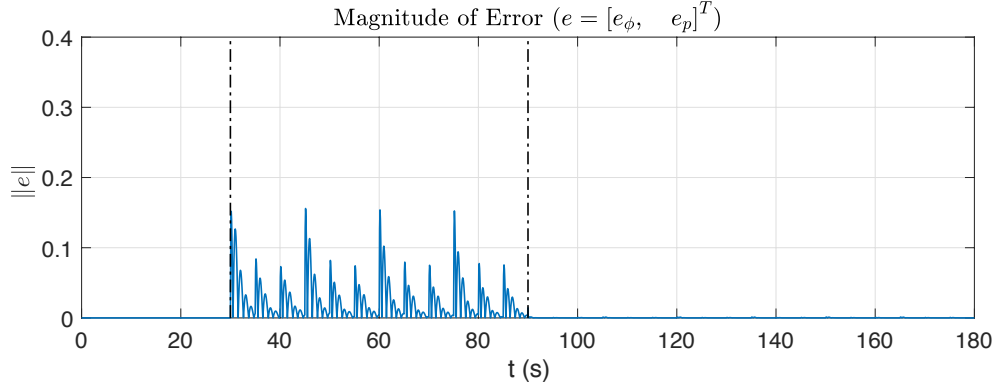


Figure 5-3: The tracking error  $e$  for the same simulation example as in Figure 5-1: under nominal operation ( $t \leq 30$  s), after the change in actuator dynamics ( $30 \text{ s} < t \leq 90$  s), and after a corrective action to switch the controller ( $t > 90$  s)

formance without requiring any manual control from the human pilot. The action required from the human pilot is in the detection and diagnosis of the anomaly in dynamical behavior, leading to the addition of feedback on  $\hat{p}$  as a corrective action.

Taking average parameter values over time  $\Delta t$  at the end of each stage of simulation (Nominal, Post-Anomaly, Post-Correction)

$$\bar{\theta}_{t_i} = \frac{1}{\Delta t} \int_{t_{f,i}-\Delta t}^{t_{f,i}} \theta(t) dt, \quad i = [1, 2, 3] \quad (5.9)$$

$$\bar{q}_{t_i} = \frac{1}{\Delta t} \int_{t_{f,i}-\Delta t}^{t_{f,i}} q(t) dt, \quad i = [1, 2, 3] \quad (5.10)$$

with  $\Delta t = 5\text{s}$ ,  $t_f = [30, 90, 180]$  allows us to define a closed-loop frequency re-

sponse which is representative of controller performance after parameter adaptation in each stage. Figure 5-4 shows the closed-loop unit step input responses with  $(\bar{\theta}_i, \bar{q}_i)$  for  $i = [1, 2, 3]$  plotted alongside the ideal response during nominal operation, demonstrating how the characteristics of nominal operation are recovered with the adaptive controller with three feedback parameters.

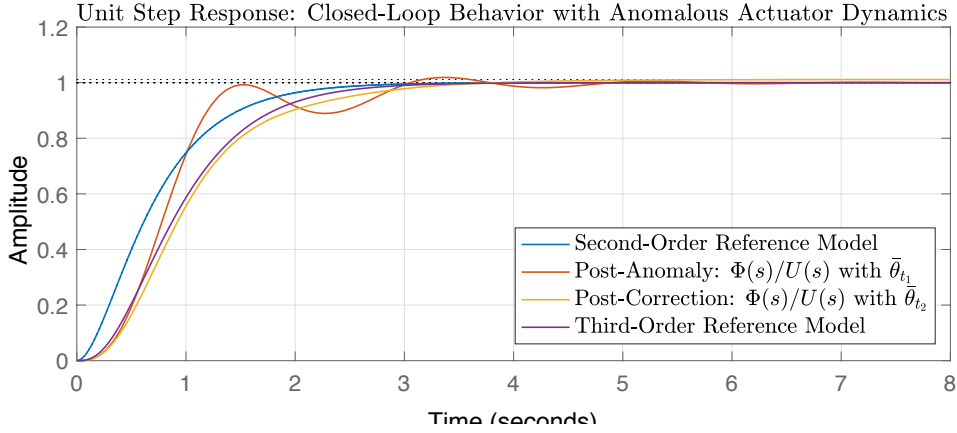


Figure 5-4: Unit step responses for closed-loop transfer functions at different stages of simulation in case (i), demonstrating performance improvement after corrective action

### 5.1.2 Time-Delayed Sensor Measurements

A time delay of  $\tau = 0.200\text{s}$  is added to the plant (3.2) between the state measurements and their use in control input computation. The reference models given by (5.3) and

$$\dot{x}'_m = \underbrace{\begin{bmatrix} 0 & 1 & 0 \\ 0 & 0 & 1 \\ -32 & -32 & -10 \end{bmatrix}}_{A'_m} x'_m + \underbrace{\begin{bmatrix} 0 \\ 0 \\ 32 \end{bmatrix}}_{B'_m} r - \underbrace{\begin{bmatrix} -10 & -1 & 0 \\ 0 & -10 & -1 \\ 32 & 32 & 9.9 \end{bmatrix}}_{L'_m} e' \quad (5.11)$$

are used in the Nominal and Post-Correction intervals, respectively. With  $\Phi_\sigma(s)$  defined as the delayed bank angle measurement, the change in the transfer function

$\Phi_\sigma(s)/U(s)$  is thus

$$\frac{\Phi_\sigma(s)}{U(s)} = \begin{cases} \frac{0.318}{s^2 + 1.10s} & t < t_{s,p} \\ \frac{0.318}{s^2 + 1.10s} e^{-0.20s} & t \geq t_{s,p} \end{cases} \quad (5.12)$$

Using the first-order delay approximation (2.8), so that  $e^{-0.20s}$  is approximated as  $1/(1 + 0.20s)$ , the feedback and feedforward gains which would give the desired closed-loop response for  $\Phi_\sigma(s)/U(s)$  are

$$\theta^*(t) = \begin{cases} \begin{bmatrix} -25.16, & -15.41 \\ -20.13, & -16.67, & -2.45 \end{bmatrix} & t < t_{s,p} \\ & t \geq t_{s,p} \end{cases} \quad (5.13)$$

$$q^*(t) = \begin{cases} 25.16 & t < t_{s,p} \\ 20.13 & t \geq t_{s,p} \end{cases} \quad (5.14)$$

The learning rates chosen for this simulation were

$$\Gamma_\theta = \begin{cases} 10I_2 & t < t_{s,c} \\ \text{diag}(10.0, 10.0, 0.1) & t \geq t_{s,c} \end{cases} \quad (5.15)$$

$$\gamma_q = 10.0 \quad \forall t \quad (5.16)$$

where the learning rate on  $\hat{p}$  is lower than that used in the simulation of case (i). This lower learning rate was needed as the approximation of the time delay as a first-order lag is fairly restrictive. In addition, a projection operator with the following constant parameters (3.15) was used to limit  $\dot{\theta}(t)$

$$\varphi_m = [300, \ 200, \ 25] \quad (5.17)$$

$$\varphi_\epsilon = [50, \ 50, \ 25] \quad (5.18)$$

and the following constant parameters for the projection operator limiting  $\dot{q}(t)$

$$\varphi_m = 300 \quad (5.19)$$

$$\varphi_\epsilon = 50 \quad (5.20)$$

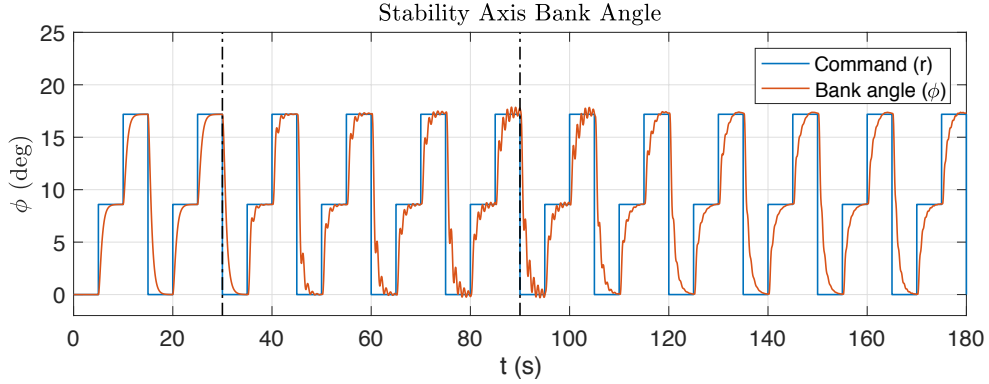


Figure 5-5: Command ( $r$ ) and output ( $\phi$ ): under nominal operation ( $t \leq 30$  s), after the sudden addition of a time delay ( $30 \text{ s} < t \leq 90 \text{ s}$ ), and after a corrective action to switch the controller ( $t > 90 \text{ s}$ )

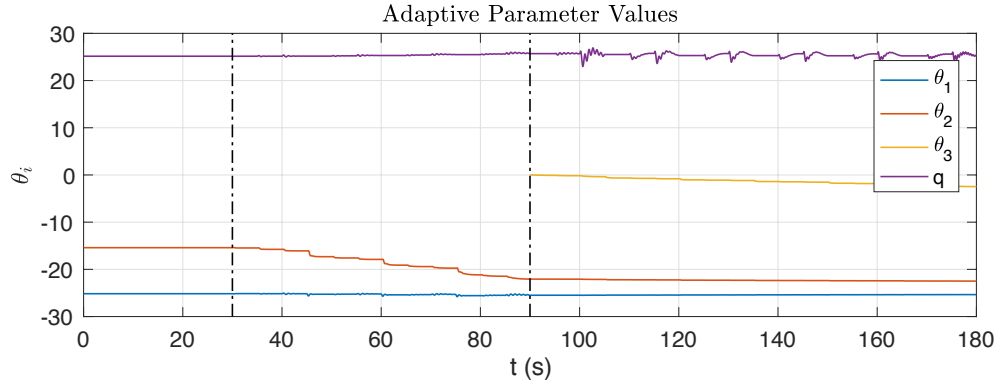


Figure 5-6: Adaptive feedback gains for the same simulation example as in Figure 5-5: under nominal operation ( $t \leq 30$  s), after the sudden addition of a time delay ( $30 \text{ s} < t \leq 90 \text{ s}$ ), and after a corrective action to switch the controller ( $t > 90 \text{ s}$ )

The resulting responses of the shared controller are shown in Figures 5-5, 5-6, and 5-7. From these results, we see that the MRAC controller with two feedback parameters has trouble tracking the commanded bank angle after the introduction of an anomaly, but the addition of a third feedback parameter ( $\hat{p}$ ) and a corresponding increase in the dimension of the reference model allows the controller to recover a

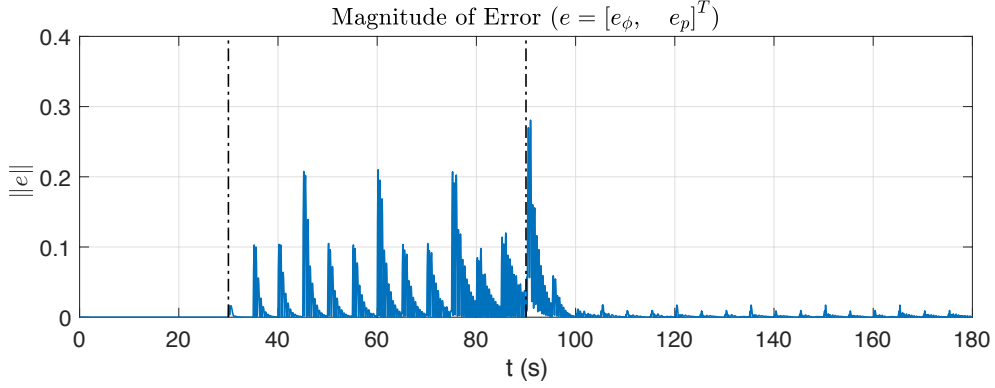


Figure 5-7: The tracking error  $e$  for the same simulation example as in Figure 5-5: under nominal operation ( $t \leq 30$  s), after the sudden addition of a time delay ( $30 < t \leq 90$  s), and after a corrective action to switch the controller ( $t > 90$  s)

reasonable tracking performance. It is worth noting that the model-following error does not converge to zero even with the MRAC controller given by (3.4), (3.11), (3.12), and (5.6), because of the time delay approximation.

The transfer functions used to generate step response plots in Figure 5-8 use (5.9) and (5.10) for average parameter values. Although the step response characteristics of Post-Correction differ more from nominal operation compared to case (i), the closed-loop response of Post-Correction is significantly more satisfactory than Post-Anomaly.

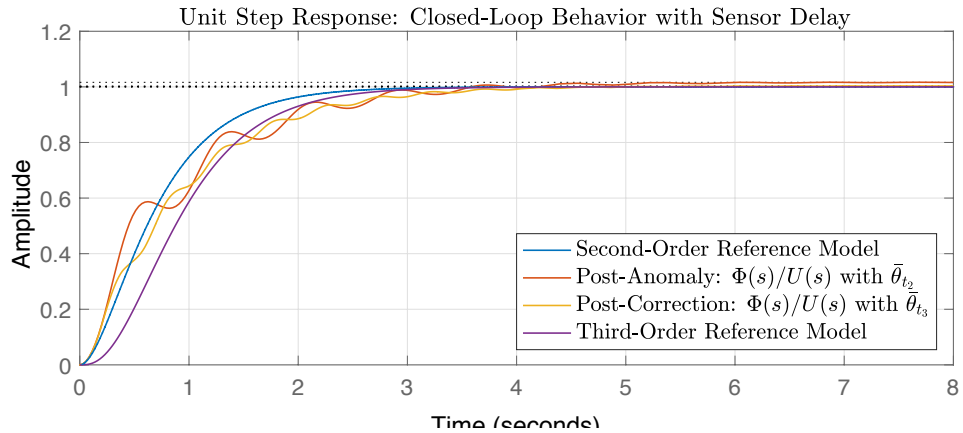


Figure 5-8: Unit step responses for closed-loop transfer functions at different stages of simulation in case (ii), demonstrating performance improvement after corrective action

The shared control solution introduced in Section ?? is applied to the problem introduced in Section 2 on a high altitude, long endurance (HALE) very flexible aircraft

(VFA) model. The aircraft model used in simulation, developed by [?] for longitudinal control design applications, is rendered in Figure 5-9 and described in Section 5.2.1. The results of numerical simulations on the control and anomaly recovery with this MIMO plant are then presented in Section 5.2.2, comparing the shared anomaly response to alternative anomaly responses.

## 5.2 Output Feedback

### 5.2.1 HALE Aircraft Model

High altitude long endurance (HALE) aerial platforms, such as the solar-electric NASA/AeroVironment Helios and Facebook Aquila, have unique design considerations to satisfy goals of uninterrupted weeks- or months-long operation. To reduce power draw, HALE aircraft designs save mass by allowing wings to bend, and may be classified as very flexible aircraft (VFA). Compared to typical fixed-wing aircraft, these aircraft operate at low speed, and may use low-bandwidth actuators which must be accounted for in control design. HALE VFA platforms are likely to have significant modeling uncertainties and online variation in dynamics due to flexible effects and degradation over long-term operation. Although these platforms are unmanned aerial vehicles (UAVs), they require supervision from remote human operators.

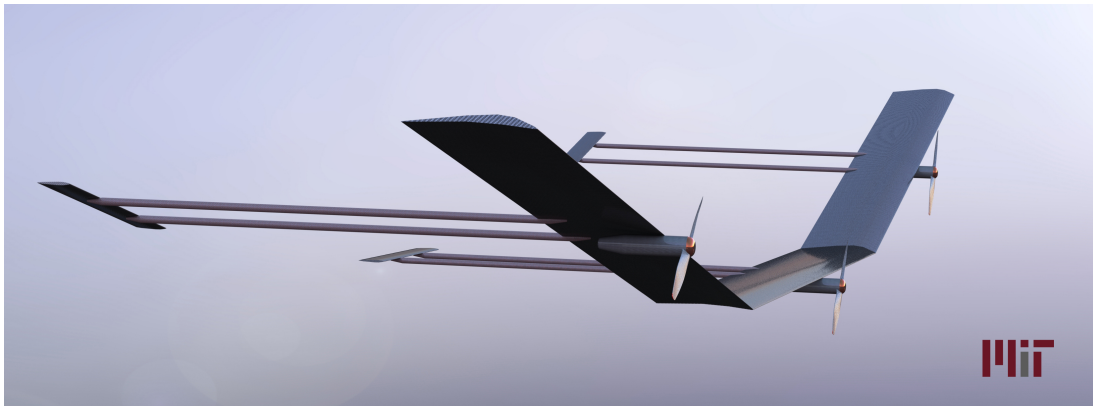


Figure 5-9: Rendering of very flexible aircraft model

The aircraft model used in simulation represents the nonlinear longitudinal dy-

namics of a HALE VFA concept with three rigid lifting sections, hinged together such that the aircraft is able to bend at the joints of the three sections. The pitch mode dynamics of this nonlinear model is defined by the state vector

$$x_{\text{vfa}} = \begin{bmatrix} V \\ \alpha \\ h \\ \theta \\ q \\ \eta \\ \dot{\eta} \end{bmatrix} = \begin{bmatrix} \text{Airspeed (ft/s)} \\ \text{Angle of attack (rad)} \\ \text{Altitude (ft)} \\ \text{Pitch angle (rad)} \\ \text{Pitch rate (rad/s)} \\ \text{Dihedral (rad)} \\ \text{Dihedral rate (rad/s)} \end{bmatrix} \quad (5.21)$$

We linearize and trim the aircraft in straight and level flight using the inputs

$$u_{\text{vfa}} = \begin{bmatrix} \delta_{th} \\ \delta_{a,c} \\ \delta_{a,o} \\ \delta_{e,c} \\ \delta_{e,o} \end{bmatrix} = \begin{bmatrix} \text{Thrust (lbf)} \\ \text{Center aileron (rad)} \\ \text{Outer aileron (rad)} \\ \text{Center elevator (rad)} \\ \text{Outer elevator (rad)} \end{bmatrix} \quad (5.22)$$

Assuming small deviations in altitude, the state vector corresponding to (2.11) is

$$x_p = [V \quad \alpha \quad \theta \quad q \quad \eta \quad \dot{\eta}]^T. \quad (5.23)$$

We consider the control task of tracking commands for the dihedral angle and vertical acceleration, using control inputs  $\delta_{a,o}$  and  $\delta_{e,c}$  only, so the vector  $u_p$  in (2.11) is

$$u_p = [\delta_{a,o} \quad \delta_{e,c}]^T. \quad (5.24)$$

Regulation of the dihedral angle is desired, as a large dihedral angle is inefficient for lift generation and introduces instability in the open-loop dynamics, while a small dihedral angle will require more control effort to hold, increasing drag and power

requirements and imparting twisting moments on the aircraft.

The measurements available for control design are the pitch rate, dihedral angle, and vertical acceleration, leading to plant outputs

$$\begin{aligned} y_p &= \begin{bmatrix} q \end{bmatrix} = \begin{bmatrix} \text{Pitch rate (rad/s)} \end{bmatrix} \\ z_p &= \begin{bmatrix} \eta \\ A_z \end{bmatrix} = \begin{bmatrix} \text{Dihedral angle (rad)} \\ \text{Vertical acceleration (ft/s)} \end{bmatrix} \end{aligned} \quad (5.25)$$

and the outputs for the augmented plant (4.2),

$$y = \begin{bmatrix} q \\ \int z_p - z_{cmd} \end{bmatrix}, \quad z = z_p. \quad (5.26)$$

For numerical simulations, the VFA model is trimmed at an airspeed of 68 ft/s, altitude of 40,000 ft, 2.8° angle of attack and pitch angle (level flight), and dihedral angles ranging from 0 to 20° in 1° increments. Figure 5-10 shows pole locations of the linearized plant for different dihedral angles, and Figure 5-11 shows instability of the linearized plant when trimmed above 11° dihedral. Figure 5-12 shows the thrust and control surface deflections for the trimmed VFA model over a range of dihedral angles.

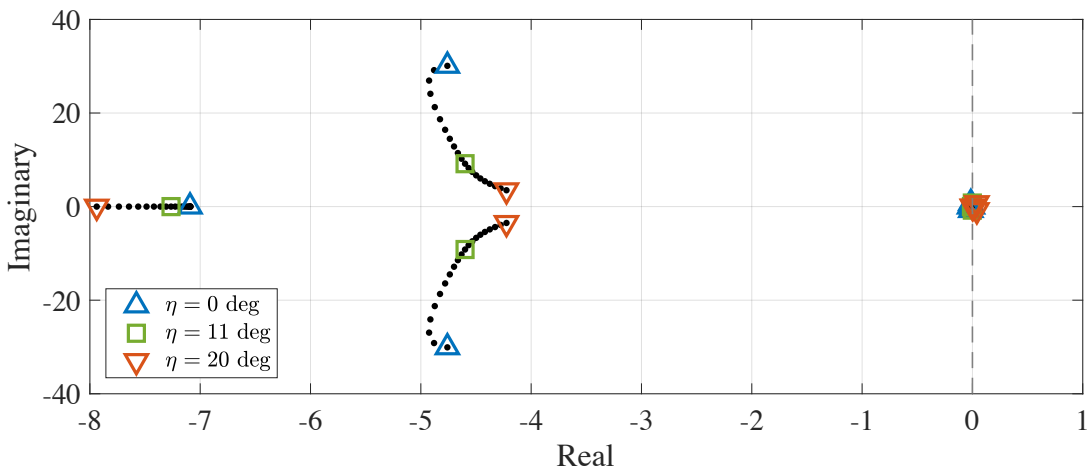


Figure 5-10: Poles of linearized system for different dihedral angles

The plant is augmented with a linear actuator model corresponding to (2.12) in

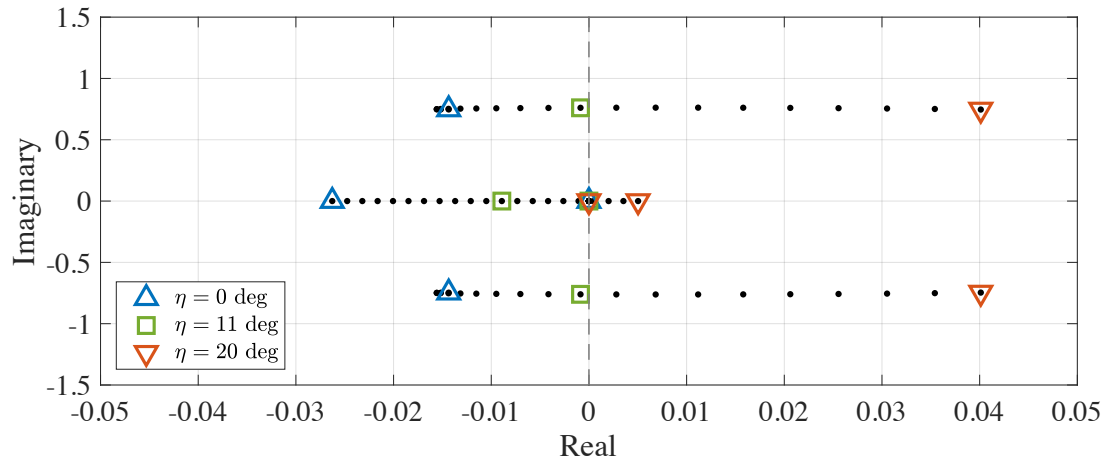


Figure 5-11: Dominant poles of linearized system, which move into the right-half complex plane when  $\eta > 11^\circ$

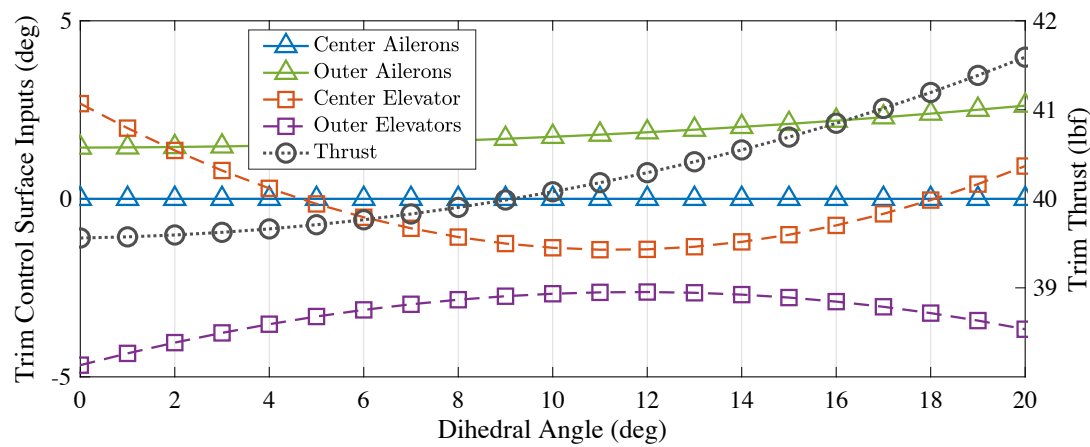


Figure 5-12: Actuator trim at different dihedral angles

the nominal case and (2.13) in the presence of anomalous dynamics. The vehicle simulation with first-order actuators (2.12) uses time constants  $(\hat{\tau}, \tau) = (0.5, 2)$ s in the control model and the actual plant, respectively, corresponding to

$$D_1 = 2I_2, \quad \Theta_1 = -1.5I_2 \quad (5.27)$$

where  $\Theta_1$  is unknown for control design, and  $I_2$  is the  $2 \times 2$  identity matrix.

Simulation of the anomalous dynamics (2.13) uses second-order actuators with cutoff frequencies  $(\hat{\omega}_c, \omega_c) = (2, 1)$  rad/s and damping ratios  $(\hat{\zeta}, \zeta) = (0.7, 0.8)$  in the control model and actual plant, respectively, corresponding to

$$\begin{bmatrix} D_1 \\ D_2 \end{bmatrix} = \begin{bmatrix} 4I_2 \\ 2.8I_2 \end{bmatrix}, \quad \begin{bmatrix} \Theta_1 \\ \Theta_2 \end{bmatrix} = \begin{bmatrix} -3.75I_2 \\ -2I_2 \end{bmatrix} \quad (5.28)$$

where  $\Theta_1$  and  $\Theta_2$  are unknown for control design. The uncertainty matrices  $\Theta_p$  and  $\Lambda$  are given by

$$\Theta_p^T = \begin{bmatrix} 0.6 & -4.52 & 0 & 0.05 & 0.41 & 1.47 \\ 0.1 & 1.83 & 0 & -0.02 & -0.35 & -0.59 \end{bmatrix} \quad (5.29)$$

$$\Lambda = 0.2I_2$$

representing a poor linearization of the nonlinear model, and an 80% reduction in actuator effectiveness.

### 5.2.2 Numerical Simulations and Results

We begin by simulating the HALE VFA under nominal autonomous control, responding to step inputs in commands for the dihedral angle and vertical acceleration, with the following three variants.

**Nom-1** Baseline RSLQR without uncertainty in control model

**Nom-2** Baseline RSLQR with uncertainty in control model ( $\Theta_p$ ,  $\Lambda_p$ , and  $\Theta_1$ )

**Nom-3** Baseline RSLQR + MRAC with uncertainty in control model ( $\Theta_p$ ,  $\Lambda_p$ , and  $\Theta_1$ )

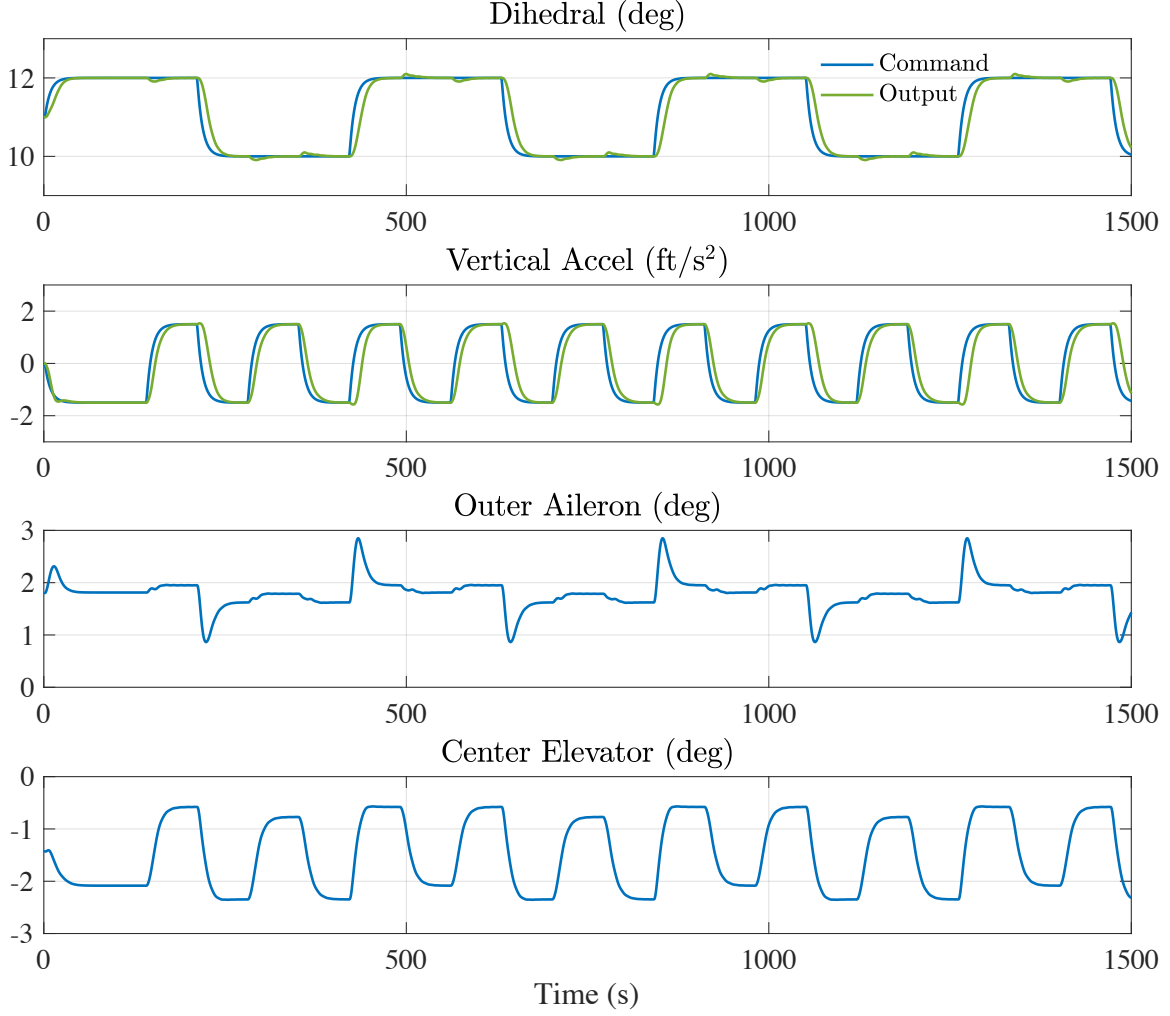


Figure 5-13: Nom-1 simulation: RSLQR with no uncertainty in the control model

These simulations, presented in Figs. 5-13, 5-14, and 5-15 respectively, show how the MRAC controller with output feedback described in (4.4)–(4.15) is able to recover the desired closed-loop performance with uncertainty in plant and actuator parameters. With the baseline RSLQR controller only, the system suffers degraded command tracking performance in the presence of uncertainty (Fig. 5-14), especially for vertical acceleration tracking.

We now simulate the introduction of a severe anomaly into the dynamics, causing the actuator dynamics to change suddenly from the uncertain first-order dynamics

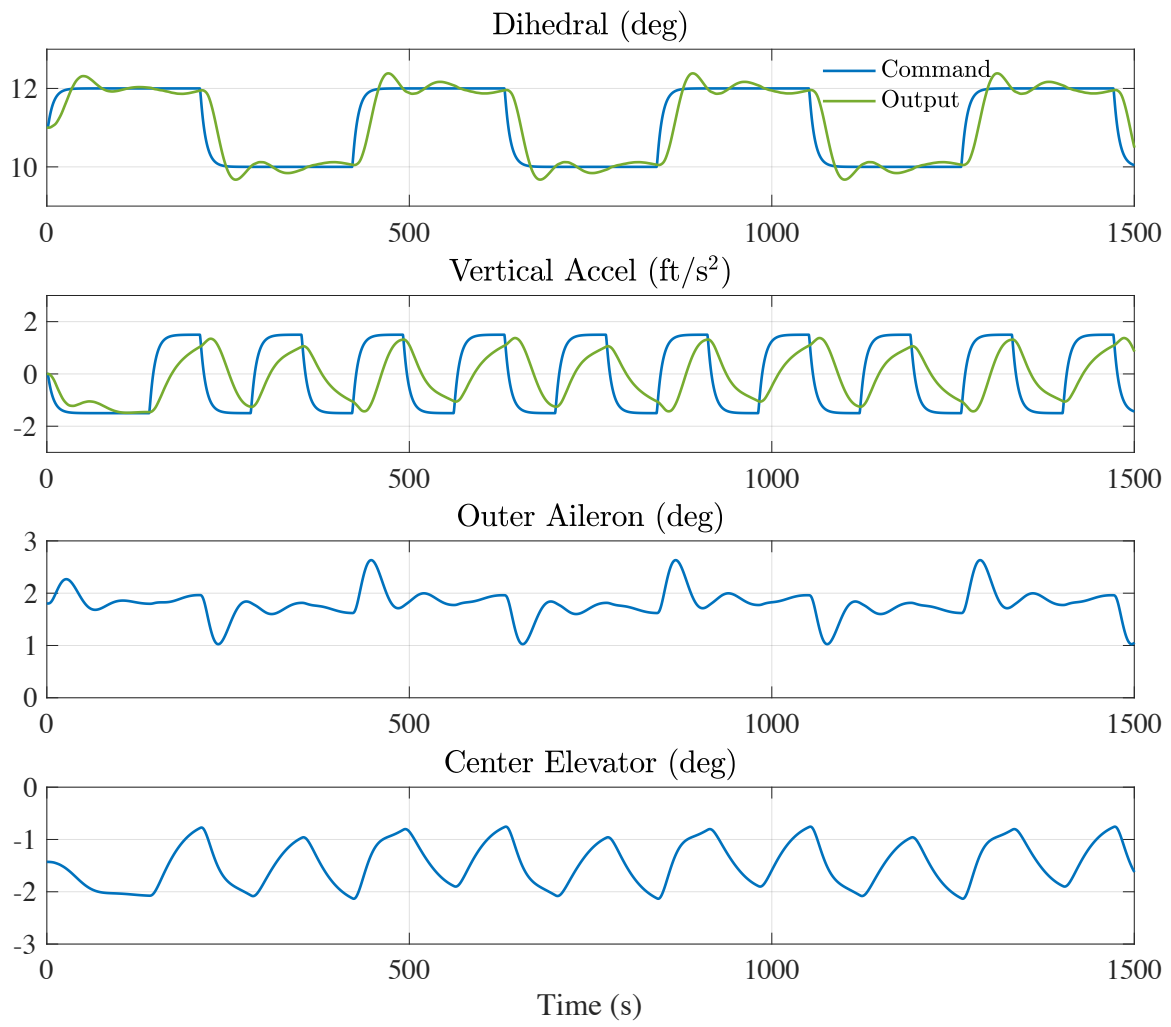


Figure 5-14: Nom-2 simulation: RSLQR with uncertainties  $\Theta_p$ ,  $\Lambda_p$ , and  $\Theta_1$

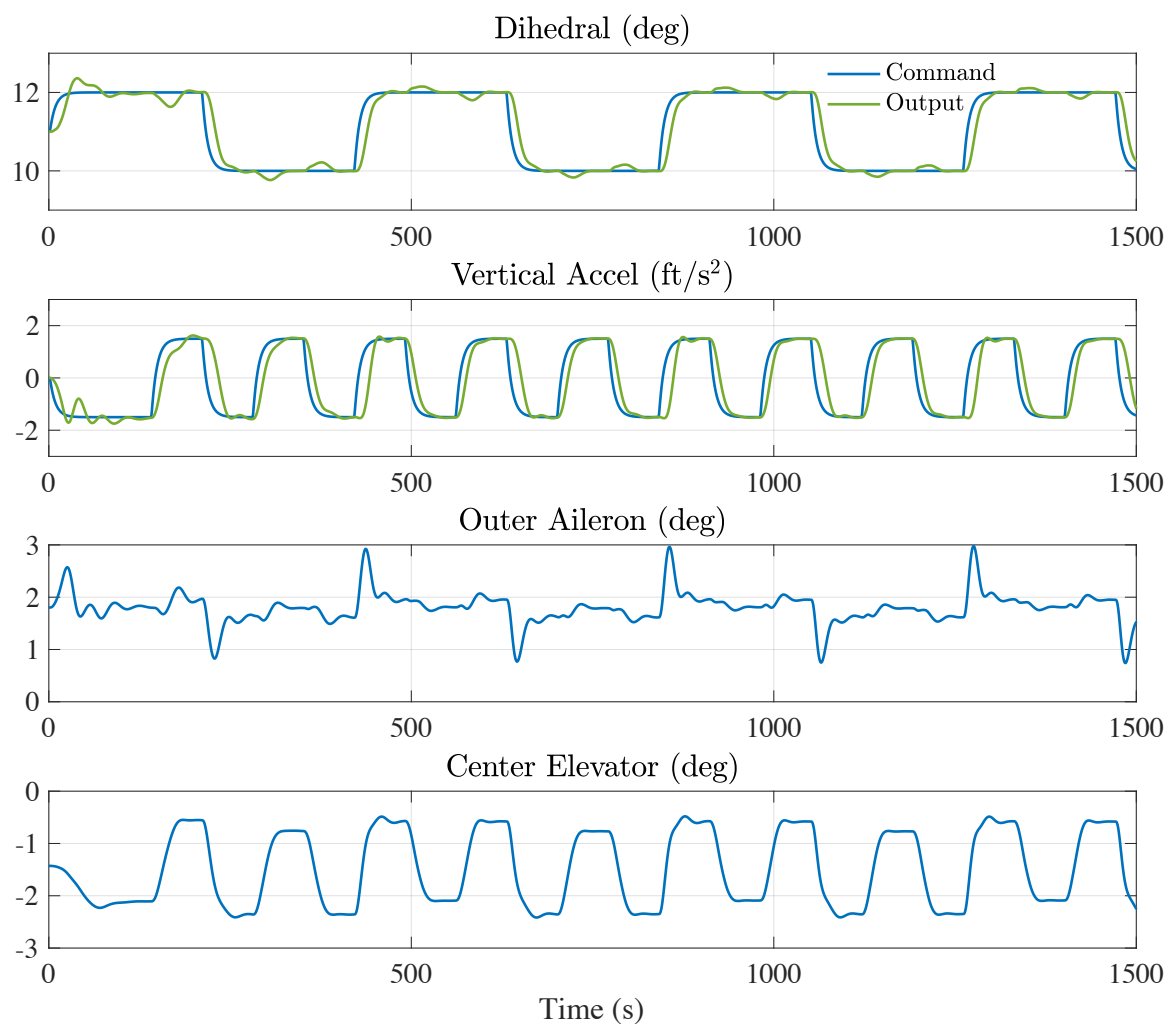


Figure 5-15: Nom-3 simulation: RSLQR + MRAC with uncertainties  $\Theta_p$ ,  $\Lambda_p$ , and  $\Theta_1$

(2.12) to the uncertain second-order dynamics (2.13). The three responses to this anomaly which we will consider are

**AR-1 (Passive)** The RSLQR+MRAC autopilot retains control without intervention from the remote human supervisor

**AR-2 (Manual)** The human operator takes over manual control of the affected vehicle

**AR-3 (Shared)** Responsibilities are shared between the human pilot and autopilot as described in Section ??

In these simulations, the vehicle operates in nominal operation with the RSLQR+MRAC control design for  $0 \leq t < 600s$ . At  $t = 600s$ , the vehicle’s actuators change from first-order (2.12) to second-order (2.13). Figs. 5-16–5-18 show the result of a passive response (AR-1) in which the human operator ignores vehicle performance degradation and allows the adaptive controller to continue operating on the plant with severely anomalous dynamics. The closed-loop system loses stability, leading to oscillations in vehicle output and eventual structural failure of the VFA at  $t = 960s$ , 6 minutes after the introduction of second-order actuator dynamics. It is worth noting the rapid increase in magnitude of the adaptive parameters and the magnitudes of both tracking and measurement output error signals after the introduction of anomalous dynamics. For comparison to a baseline without adaptive control, a passive response using only the RSLQR controller leads to structural failure following the anomaly, at  $t = 1240s$ .

Numerical simulations of the AR-2 response (purely manual control) are not carried out, as they are not deterministic and require high-fidelity *human-in-the-loop* experiments to characterize. The limitations of such a response – in which the human operator’s role changes suddenly from “on-the-loop” to “in-the-loop” with unfamiliar dynamics – are discussed in the earlier sections of this paper.

Results of the AR-3 (shared control) anomaly response simulation are shown in Figs. 5-19–5-21. After the anomaly is introduced at  $t = 600s$ , the “nominal” controller attempts to control the system whose dynamics are not fully accounted for in the

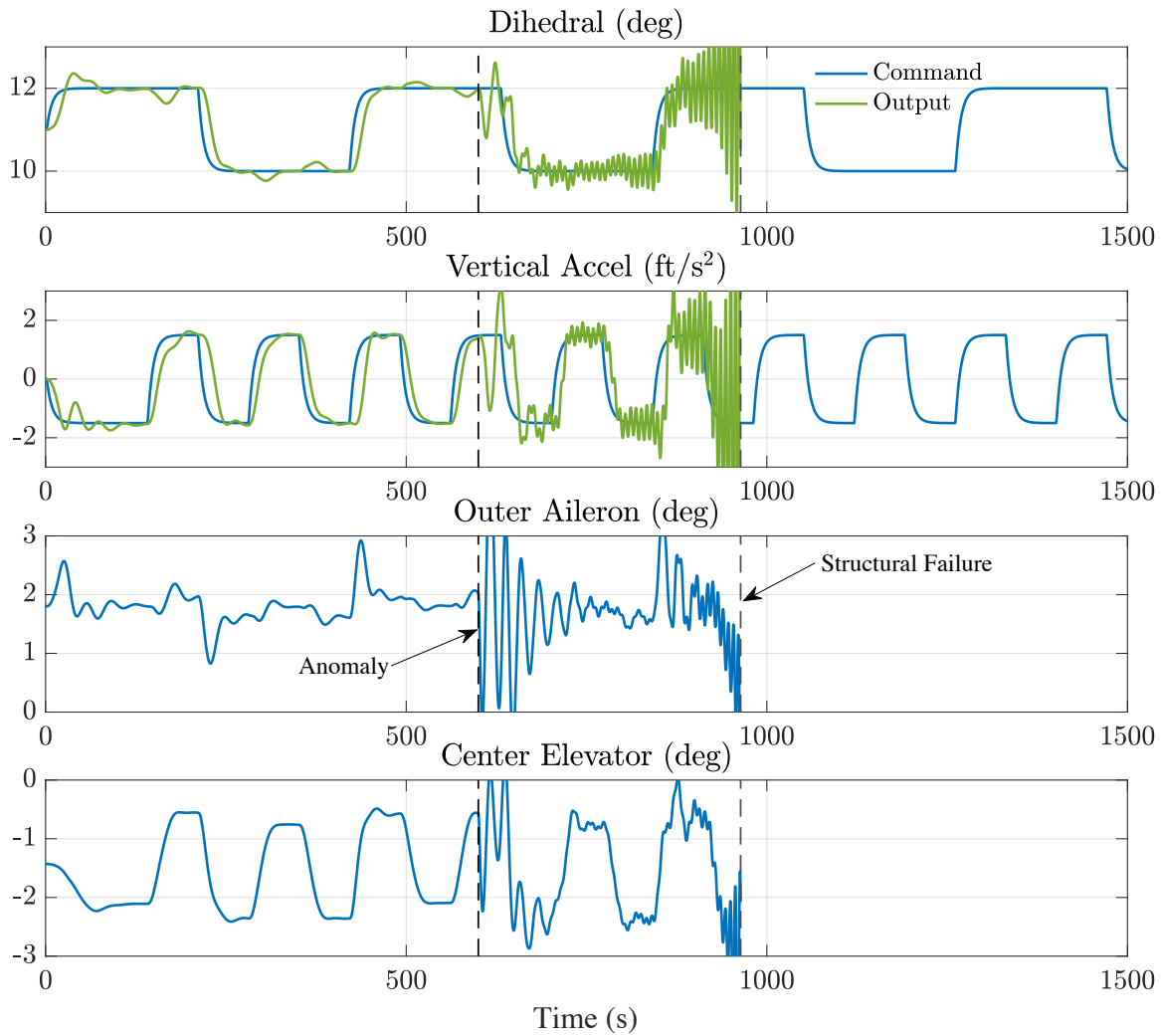


Figure 5-16: AR-1 simulation: passive response to dynamical anomaly results in structural failure after 6 minutes

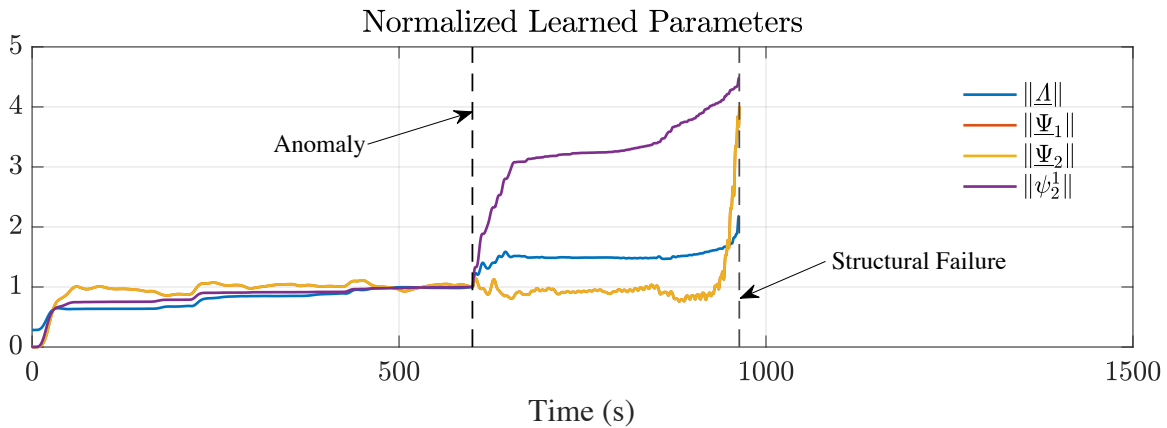


Figure 5-17: AR-1 simulation: adaptive parameters diverge as controller struggles to adapt to unmodeled dynamics

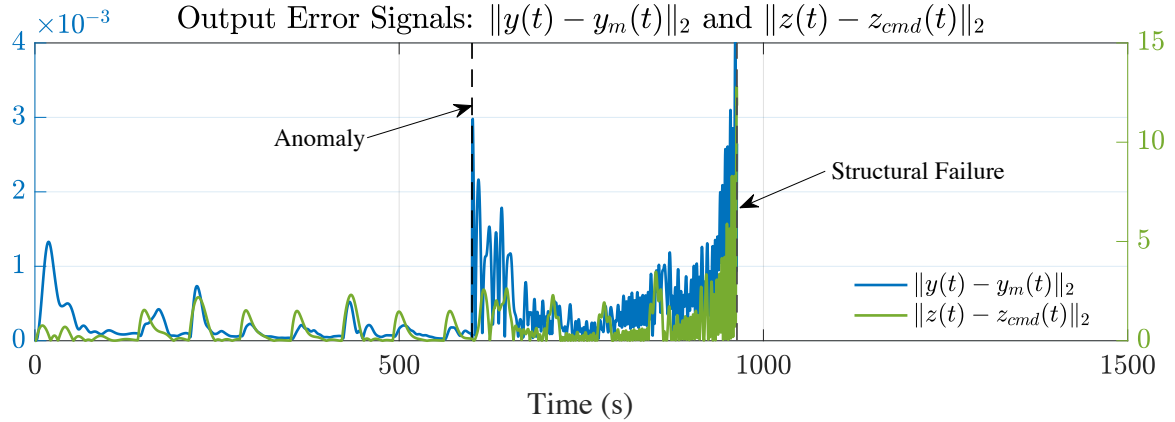


Figure 5-18: AR-1 simulation: model-following output error and command tracking error grow due to anomalous dynamics

control model. Simultaneously in the shared control framework, the human operator notices the anomalous closed-loop control behavior, and via an interface switches the controller to the higher relative degree design (4.16)–(4.34) at  $t = 800s$ , which is the culmination of the human operator’s action. For  $t \geq 800s$ , the vehicle remains under autonomous control with the “recovery” adaptive controller and is able to reestablish nominal command tracking performance. For comparison, the time of structural failure in the passive anomaly response is plotted as a line at  $t = 960s$ .

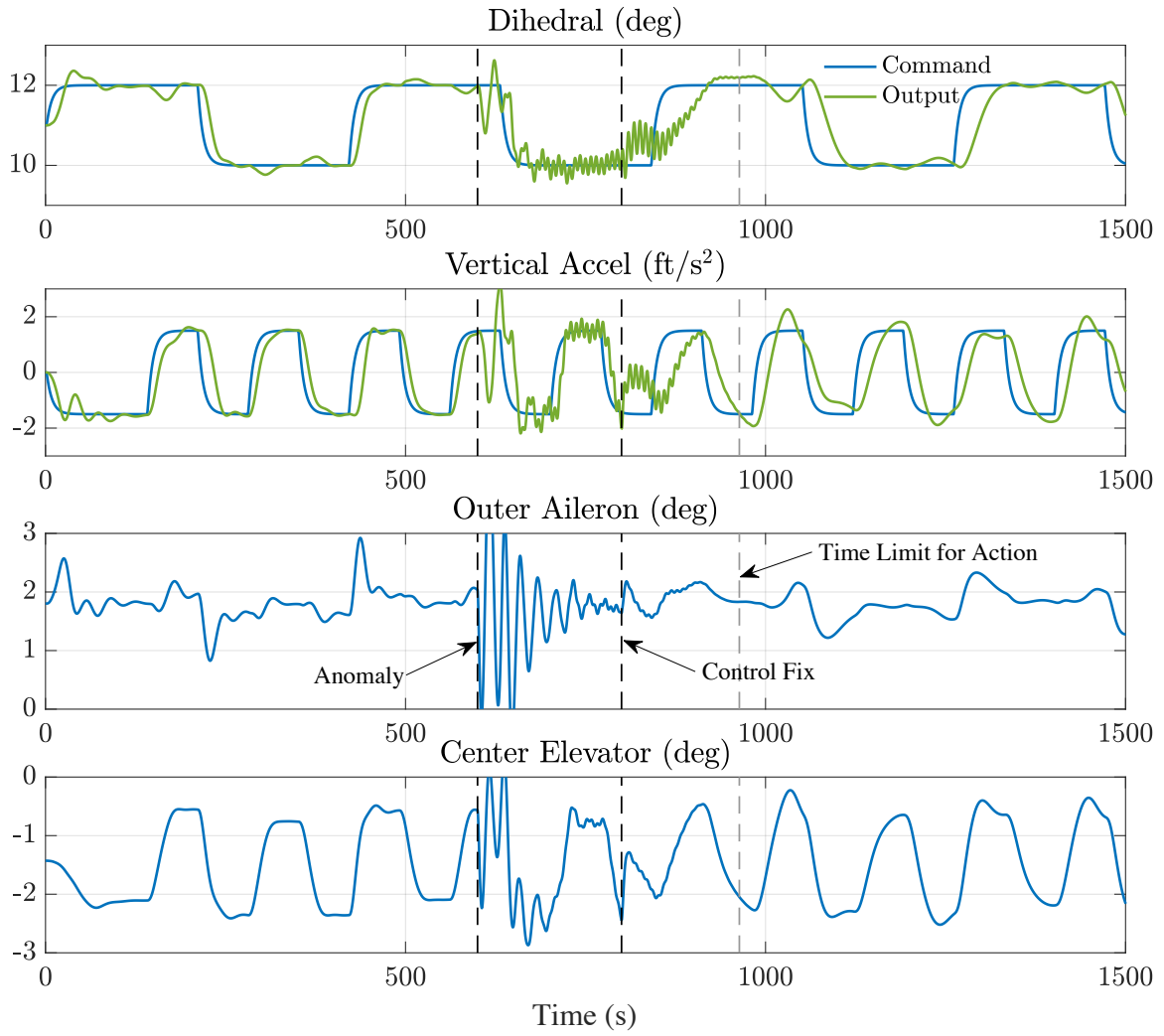


Figure 5-19: AR-3 simulation: shared response to the dynamical anomaly results in recovery of vehicle performance

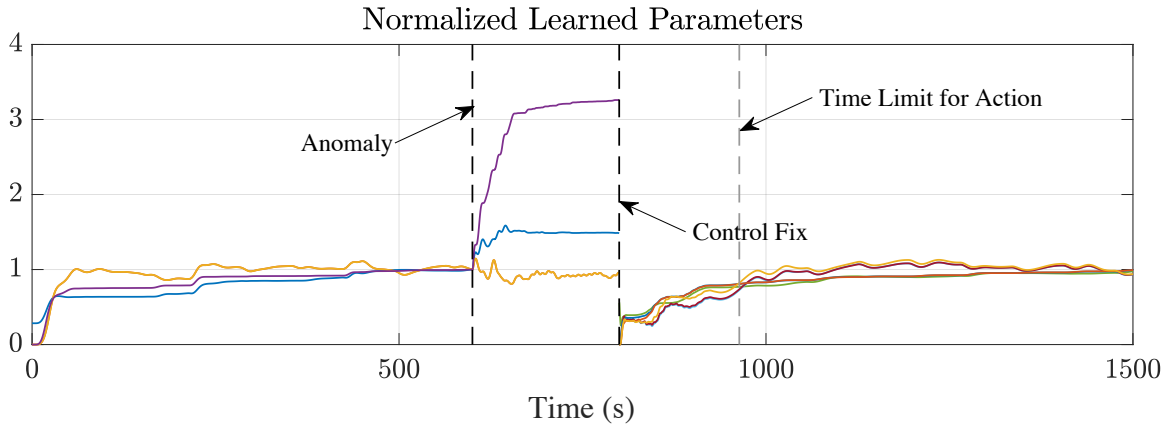


Figure 5-20: AR-3 simulation: the change in control model at  $t = 800s$  stops the divergence of adaptive parameters

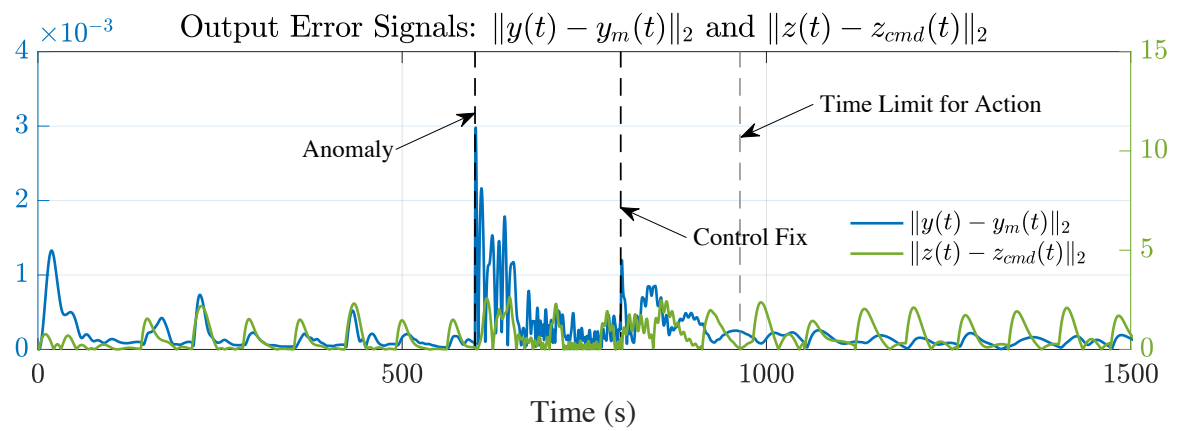


Figure 5-21: AR-3 simulation: the change in control model at  $t = 800s$  stops the error growth seen after the anomaly



# Chapter 6

## Concluding Remarks

This work develops a shared control framework between adaptive autopilots and remote human operators of aerial vehicles. The autonomous control design (autopilot) builds on two recent advances in adaptive control theory, namely the use of closed-loop reference models for improved transient performance, and computationally efficient control designs for output-feedback systems having relative degree two or greater. The targeted role of the human operator is motivated by unmanned aerial platforms remotely supervised by humans (“human-on-the-loop”), and the limitations that come with remote manual control. Under our shared control framework, the human operator and adaptive autopilot designs form a shared response to dynamical anomalies. The shared control response is demonstrated in simulation on the longitudinal dynamics of an unmanned HALE VFA model.

When human pilots are suddenly presented with unfamiliar dynamics, they attempt to adapt their feedback gains, but performance deteriorates which increases the potential for loss of control events. Autonomous adaptive controllers present the potential to remove the human pilot from low-level control tasks and instead allow them to make high-level decisions, such as the switching of the controller structure to a suitable dimension which allows the adaptive autopilot to retain autonomous control of the vehicle. The human pilot collaborates with the autopilot in the detection and diagnosis of the anomaly and relegates corrective actions to an adaptive flight control system. As an autonomous adaptive flight control system will be able

to control these low-level tasks with ease, such a shared controller may prove to be more advantageous in the face of severe anomalies.

We explore the behavior of a shared controller in the context of the roll dynamics of an aircraft, in the face of two different kinds of anomalies. In both cases, the pilot's task is to perceive if there is a change in the order of the vehicle dynamics, and convey this change to the adaptive autopilot. The resulting shared control action was shown to lead to satisfactory performance through detailed simulation studies.

To further develop the shared control architecture, more detailed perception models of the human will need to be derived and evaluated using realistic vehicle models and scenarios. Additionally, algorithms based on human perception models may be developed to aid in autonomous anomaly detection. These form the subject of future work.

# Appendix A

## Tables

Table A.1: Armadillos

Armadillos	are
our	friends